Statistical characterization of erosion and sediment transport mechanics in shallow tidal environments. Part 2: suspended sediment dynamics

Davide Tognin[1,2], Andrea D'Alpaos[2], Luigi D'Alpaos[1], Andrea Rinaldo[1,3], and Luca Carniello[1]

[1]Department of Civil, Environmental, and Architectural Engineering, University of Padova, Padova, Italy
[2]Department of Geosciences, University of Padova, Padova, Italy
[3]Laboratory of Ecohydrology ECHO/IEE/ENAC, Ècole Polytechnique Fèdèrale de Lausanne, Lausanne, Switzerland

Correspondence: Davide Tognin (davide.tognin@unipd.it)

Abstract. A proper understanding of sediment resuspension and transport processes ~~dynamics , critically including resuspension and deposition processes of suspended sediments,~~ is key to the morphodynamics of shallow tidal environments. However, a complete spatial and temporal coverage of suspended sediment concentration (SSC) to describe these processes is hardly available, preventing the effective representation of depositional dynamics in long-term modelling approaches. ~~Aiming to account for deposition mechanics in a synthetic theoretical framework introduced to model erosion dynamics (D'Alpaos et al., 2023), here we investigate suspended sediment dynamics.~~ Aiming to couple erosion and deposition dynamics in a unique synthetic theoretical framework, here we investigate SSC dynamics following a similar approach to that adopted for erosion (D'Alpaos et al., 2023). ~~A complete spatial and temporal coverage of suspended sediment concentration (SSC) required to effectively characterize resuspension events is hardly available through observation alone, even combining point measurements and satellite images, but it can be retrieved by properly calibrated and tested numerical models. We analyzed one-year-long time series of SSC computed by a bi-dimensional, finite-element model in six historical configurations of the Venice Lagoon in the last four centuries. Following the peak-over-threshold theory, we statistically characterized suspended sediment dynamics by analyzing interarrival times, intensities and durations of over-threshold SSC events.~~ The analysis with the peak-over-threshold theory of SSC time series computed using a fully-coupled, bi-dimensional model allows us to identify interarrival times, intensities and durations of over-threshold events and test the hypothesis of modelling SSC dynamics as a Poisson process. The effects of morphological modifications on spatial and temporal SSC patterns are investigated in the Venice Lagoon, for which several historical configurations in the last four centuries are available. Our results show that, similarly to erosion events, SSC can be modelled as a marked Poisson process in the intertidal flats for all the analysed morphological lagoon ~~considered historical~~ configurations ~~of the Venice Lagoon~~ because exponentially distributed random variables well describe ~~interarrival times, intensity and duration of~~ over-threshold events. ~~Moreover, interarrival times, intensity and duration describing local erosion and over-threshold SSC events are highly related, although not identical because of the non-local dynamics of suspended sediment transport related to advection and dispersion processes. Owing to this statistical characterization of SSC events, it is possible to generate synthetic, yet realistic, time series of SSC for the long-term modelling of shallow tidal environments.~~ Although erosion and resuspension are intimately intertwined, erosion alone does not suffice to describe also SSC because of the non-local

25 dynamics due to advection and dispersion processes. The statistical characterization of SSC events completes the framework introduced for erosion mechanics and, together, they represent a promising tool to generate synthetic, yet realistic, time series of shear stress and SSC for the long-term modelling of tidal environments.

1 Introduction

Suspended sediment dynamics in shallow tidal systems play a significant role as they influence geomorphic and ecological
30 processes, that ultimately determine the long-term morphodynamic evolution of coastal, estuarine and lagoonal landscapes (Woodroffe, 2002; Masselink et al., 2014). Physical processes that drive sediment resuspension and transport in tidal environments are influenced by different hydrodynamic and sedimentological factors over a wide range of spatial and temporal scales.

Both tide and waves represent key drivers controlling sediment entrainment and transport in shallow tidal environments
35 (Wang, 2012). The tide rise and fall generate currents that propagate along the preferential pathways provided by the channel network (Hughes, 2012) but, as the tide overspills on the adjoining intertidal flats, it is strongly affected by shallower water and friction effects (Friedrichs and Madsen, 1992), so that its velocity and, hence, its resuspension capacity can diminish considerably. Whereas, wind waves with a typically short period can generate wave-orbital motions capable of resuspending intertidal-flat sediments (Anderson, 1972; Dyer et al., 2000; Carniello et al., 2005; Green, 2011). Therefore, stochastic wave-
40 forced resuspension can increase locally, mainly under storm conditions, and can overcome the cyclic resuspension by tidal currents in generating high turbidity (Green et al., 1997; Ralston and Stacey, 2007; Sanford, 1994). Wave-driven resuspension and erosion together with tide- and wave-driven sediment transport give rise to mechanisms leading to basin-wide sediment movement, which strongly shape the morphology of shallow tidal systems (e.g., Nichols and Boon, 1994; Green and Coco, 2007; Carniello et al., 2011; Green and Coco, 2014). The repeated cycles of erosion, resuspension and deposition, that sedi-
45 ments may undergo, winnow fine particles from coarser ones and, thus, modify sediment distribution and textural properties of intertidal flats and subtidal platforms, influencing physical and biological processes (Dyer, 1989), light climate (Moore and Wetzel, 2000) and ecosystem productivity (Carr et al., 2010; Lawson et al., 2007; Carr et al., 2016; McSweeney et al., 2017).

Moreover, resuspension dynamics are mutually linked to numerous biological and ecological processes (Temmerman et al., 2007; Kirwan and Murray, 2007; D'Alpaos et al., 2007, 2011; Marani et al., 2013). Benthic vegetation and algae play a key
50 role in increasing sediment stability of subtidal platforms (Nepf, 1999; Tambroni et al., 2016; Venier et al., 2014). In fact, the interaction of flexible vegetation and bedforms can reduce the effective bed shear stress and, consequently, sediment mobility. Similarly, the action of halophytic vegetation over salt marshes has a significant impact on landscape development, enhancing accretion, both by directly trapping inorganic sediment and by producing organic matter (Marani et al., 2013; D'Alpaos and Marani, 2016; Roner et al., 2016; Puppin et al., 2023). However, some studies have also suggested that, although vegetation an-
55 chors sediment through rooting and by slowing water flows, erosion and scour of the proximal sediments can also be enhanced (Temmerman et al., 2007; Tinoco and Coco, 2016). Microalgae, although small, may also heavily impact sediment erodibility. Indeed, extracellular polymeric secretions (EPS) of microphytobenthos can increase grain adhesion and consequently erosion

threshold of the sedimentary substrate (Le Hir et al., 2007; Parsons et al., 2016; Chen et al., 2019). As a result, sediment resuspension decreases in the presence of EPS, which affects light availability and, in turn, microalgae proliferation, thus triggering positive feedback (Pivato et al., 2019). Benthic fauna can further modify the bed sediment by changing its geotechnical properties and erosion resistance (Widdows and Brinsley, 2002; Vu et al., 2017). Owing to the complexity of the underlying processes and the interplay between physical and biological drivers, sediment dynamics in shallow tidal systems are rather entangled.

Several numerical models have been developed to describe sediment transport and different techniques have been proposed to upscale the effects on the morphological evolution of tidal systems. For instance, explorative point-based models are extensively used to understand the relative importance of sediment transport processes, because of their simplified parametrization as well as their great conceptual value (Murray, 2007). Furthermore, their reduced computational burden is ideal to investigate trends over long-term time scales. For these reasons, point-based models have been largely adopted, for example, to examine salt-marsh fate under different sea level rise scenarios at the century time scale (D'Alpaos et al., 2011; Fagherazzi et al., 2012). However, point-based models potentially miss spatial dynamics associated with sediment transport and, hence, might fail to represent interactions between different morphological units. More detailed, process-based models can fill this gap and account for sediment fluxes between different points up to the whole basin scale (e.g. Lesser et al., 2004; Carniello et al., 2012). But, because of the explicit description of the short-term interaction between hydrodynamics and sediment transport, the application of process-based models to the long-term time scale is often computationally expensive or even prohibitive. A widespread solution to overcome this limitation is to upscale the effects of short-term sediment transport on bed evolution by means of the so-called 'morphological factor', basically a multiplication factor to accelerate the computation of the effects on the morphology (Lesser et al., 2004; Roelvink, 2006).

These approaches implicitly assume that the morphological response of a system in the long term can be directly upscaled from the bed-level changes explicitly computed using a representative forcing condition on a much shorter time scale. However, as soon as the morphological evolution of a system is substantially affected by stochastic, episodic events, namely wind waves and storm surges (Tognin et al., 2021), and, therefore, cannot be represented as a continuous process (i.e. purely driven by the tide), this assumption may provide misleading results. Moreover, in tidal systems with fine sediments, because of the effect of consolidation, stratification and armouring of the sediment bed (Mehta et al., 1989), the morphological response is usually critically influenced by the magnitude and the time-history of events (Mathew and Winterwerp, 2022), which obviously cannot be reproduced by considering simplified, repetitive forcing conditions.

To explicitly model the effects of stochastic, morphologically-meaningful events as well as their temporal succession, a possible alternative would be to directly consider the physical processes responsible for the morphological evolution (i.e. erosion, transport and deposition of sediment) instead of upscaling the bed level changes. From this perspective, synthetic, statically-based models represent a particularly promising framework to reduce the computation burden associated with the explicit description of these processes through the use of independent Monte Carlo realizations. Notwithstanding the increasing popularity of statistically-based approaches for long-term modelling in hydrological and geomorphological sciences (e.g., Rodriguez-Iturbe et al., 1987; D'Odorico and Fagherazzi, 2003; Botter et al., 2013; Park et al., 2014), applications to tidal systems are still quite unusual (D'Alpaos et al., 2013; Carniello et al., 2016).

In order to explicitly describe sediment transport and bed evolution in a statistically-based framework, two different complementary processes need to be characterized: bottom shear stress (BSS), which can be considered a proxy for erosion, and suspended sediment concentration (SSC), which represents a measure of the sediment potentially available for deposition. To this goal, the characterization of BSS is provided by D'Alpaos et al. (2023). Here we aim to complete the proposed framework by statistically characterizing SSC and testing the possibility to describe suspended sediment dynamics as a Poisson process in long-term morphodynamic models.

~~Therefore, observation-based approaches have been widely adopted to investigate the suspended sediment concentration (hereafter SSC), using either in situ point measurements (e.g., Wren et al., 2000; Gartner, 2004; Brand et al., 2020) or remote sensing and satellite image analysis (Miller and McKee, 2004; Ruhl et al., 2001; Volpe et al., 2011).~~

SSC dynamics is usually characterized either by in situ point measurements (e.g., Wren et al., 2000; Gartner, 2004; Brand et al., 2020) or by remote sensing and satellite image analysis (Miller and McKee, 2004; Ruhl et al., 2001; Volpe et al., 2011). However, both these techniques have some drawbacks and do not offer the proper spatial and temporal coverage required for the statistical characterization. In situ measurements can provide an accurate description of the temporal dynamics of SSC, but lacks information on its spatial heterogeneity. Moreover, acoustic and optical sensors installed in point turbidity stations require periodic cleaning to prevent failure due to biofouling. Whereas, satellite-based data can supply instantaneous information on SSC spatial variability, but are barely informative on its temporal dynamics. Indeed, SSC events can hardly be fully captured by satellites with fixed and often long revisit periods. Furthermore, intense SSC typically occurs during severe storms, frequently characterized by clouds, which make satellite data useless. As a matter of fact, reliable long-term SSC time series at the basin scale, required for the statistical analysis performed herein, are seldom available. In order to overcome these shortcomings and to exploit measurements of in situ point observations and satellite images, these data can be combined to calibrate and test numerical models (Ouillon et al., 2004; Carniello et al., 2014; Maciel et al., 2021), thereby, using them as physically-based "interpolators" to compute temporal and spatial SSC dynamics required by this analysis. ~~However, computing SSC dynamics over time scales of centuries in order to model the morphodynamic evolution of tidal environments through fully-fledged numerical models is rather difficult owing to the computational burden involved. Therefore, modelling the long-term evolution of tidal systems requires comprehending the physics of the processes in order to properly characterize them in the framework of simplified approaches (Murray, 2007). Pointing to the development of a synthetic theoretical framework to represent intense SSC events and to account for their landscape-forming action on tidal basin morphology, we applied a two-dimensional finite element model to simulate the interaction among wind waves, tidal current and sediment transport in several historical configurations of the Venice Lagoon. Here~~In particular, we used a previously-calibrated and widely-tested Wind Wave-Tidal Model (WWTM) (Carniello et al., 2005, 2011) coupled with a sediment transport model (Carniello et al., 2012) to investigate SSC dynamics.

This study aims to verify if the proposed framework can be properly applied over long-term time scales and, hence, is independent of the specific morphological setting of a tidal basin. Hence, we perform the analysis on the Venice Lagoon, Italy (Figure 1), for which several historical morphological configurations are available in the last four centuries (Carniello et al., 2009; D'Alpaos, 2010; Finotello et al., 2023). In particular, we considered ~~to investigate hydrodynamics and suspended~~

sediment dynamics in the following six historical configurations of the Venice Lagoon : 1611, 1810, 1901, 1932, 1970, and 2012. For each of them, we run a one-year-long simulation forced with representative tidal and meteorological boundary conditions. The computed SSC time series have been analyzed on the basis of the peak-over-threshold (POT) theory, following the approach introduced by D'Alpaos et al. (2013) and expanding the analysis performed by Carniello et al. (2016) to study the statistics of SSC in the present configuration of the Venice Lagoon. This study aims to expand this analysis to other historical configurations of the Venice Lagoon (Figure 1) in order to unravel the effects on sediment transport of the morphological and anthropogenic modifications experienced by the lagoon in the last four centuries and to test whether SSC dynamics can be modelled as a marked Poisson process also when accounting for the morphological evolution of the basin. The latter represents an interesting goal, being the use of stochastic frameworks particularly promising for long-term studies, as pointed out by their increasing popularity in hydrology and geomorphology to describe the long-term behaviour of geophysical processes (e.g., Rodriguez-Iturbe et al., 1987; D'Odorico and Fagherazzi, 2003; Botter et al., 2013; Park et al., 2014; Bertassello et al., 2018) Nonetheless, applications to tidal systems are still quite uncommon (D'Alpaos et al., 2013; Carniello et al., 2016). Our analysis provides a spatial and temporal characterization of resuspension events for the Venice Lagoon from the beginning of the seventeenth century to the present day, in order to show how morphological modifications affected sediment transport and to set up a stochastic framework to forecast future scenarios.

2   Materials and Methods

The Venice Lagoon (Figure 1) underwent different morphological changes over the last four centuries, mainly associated with in particular due to anthropogenic modifications (Carniello et al., 2009; D'Alpaos, 2010; Finotello et al., 2023). From the beginning of the fifteenth century, the main rivers (Brenta, Piave, and Sile) were gradually diverted in order to flow directly into the sea and prevent the lagoon from silting up, but this triggered the present-daya sediment starvation condition. Later, during the last century, The inlets were provided with jetties between 1839 and 1934 and deep navigation channels were excavated to connect the inner harbour with the sea between 1925 and 1970 (D'Alpaos, 2010). The jetties deeply changed the hydrodynamics at the inlets establishing an asymmetric hydrodynamic behaviour responsible for a net export of sediment toward the sea after their construction (Martini et al., 2004; Finotello et al., 2023), especially during severe storm events, which are responsible for the resuspension of large sediment volumes (Carniello et al., 2012). In general, these modifications , together with sea level rise, heavily influenced sediment transport triggering strong erosion processes in the following period. that were further aggravated by sea-level rise. The net sediment loss clearly emerges from the comparison among the different surveys of the Venice Lagoon, which show a generalized deepening of tidal flats and subtidal platforms as well as a reduction of salt-marsh area (Carniello et al., 2009). Indeed, in the last century, the average tidal-flat bottom elevation lowered from -0.51 m to -1.49 m above mean sea level (a.m.s.l.), while the salt-marsh area progressively shrank from 164.36 km^2 to 42.99 km^2 (Tommasini et al., 2019). This erosive trend displays a relative slowdown in the last 30 years because of the larger hydrodynamic forcing required to rework bed sediment at an increasing water depth (Finotello et al., 2023). HoweverMoreover, repeated closures of storm-surge barriers designed to protect the city of Venice from flooding and known as Mo.S.E. system are expected to further

exacerbate this morphological degradation by cutting off significant supplies of inorganic sediments brought in by intense storm-surge events (Tognin et al., 2022). As a result, the morphological evolution of the lagoon in the last four centuries has been strongly affected by anthropogenic interventions, along with sea level rise.

To study the influence of these morphological changes on suspended sediment dynamics, we considered six different historical configurations of the Venice Lagoon, ranging from the beginning of the seventeenth century to today (Figure S1). The three most ancient configurations (i.e. 1611, 1810, and 1901) were modelled by relying on historical maps, whereas the topographic surveys carried out by the Venice Water Authority (Magistrato alle Acque di Venezia) in 1932, 1970, and 2003 were used for the more recent ones (D'Alpaos, 2010; Finotello et al., 2023). Due to some morphological modifications at the three inlets associated with the Mo.S.E. system and almost completed in 2012, the 2003 configuration was updated, so we will refer to this configuration as the 2012 configuration. Each bathymetry and, hence, the elevation of grid elements refers to the local mean sea level at the time when each survey was performed. For a detailed description of the methodology applied for the reconstruction of the historical configurations of the Venice Lagoon and additional information on the more recent bathymetric data, we refer the reader to Tommasini et al. (2019). Further details on the geomorphological setting and the implications on erosion and resuspension events are reported in D'Alpaos et al. (2023).

2.1 Numerical Model

The flow field and sediment transport in the six configurations of the Venice Lagoon are computed by using a numerical model, consisting of three modules. The coupling of the hydrodynamic module with the wind-wave module (WWTM) describes the hydrodynamic flow field together with the generation and propagation of wind waves (Carniello et al., 2005, 2011), while the sediment transport and the bed evolution module (STABEM) evaluates the sediment dynamics and the effects on the morphology (Carniello et al., 2012). All modules share the same computational grid.

The hydrodynamic module solves the 2-D shallow water equations using a semi-implicit staggered finite element method based on Galerkin's approach (Defina, 2000). The equations are suitably rewritten in order to deal with flooding and drying processes in morphologically irregular domains. The Strickler equation is used to evaluate the bottom shear stress induced by currents, τ_c, considering the case of turbulent flow over a rough wall. Moreover,Further, the hydrodynamic module provides the flow field characteristic usedrequested by the wind-wave module to simulate the generation and propagation of wind waves.

The wind-wave module (Carniello et al., 2011) solves the wave action conservation equation parametrized using the zero-order moment of the wave action spectrum in the frequency domain (Holthuijsen et al., 1989). The peak wave period is related to the local wind speed and water depth, and this empirical correlation function is used to determine the spatial and temporal distribution of the wave period The spatial and temporal patterns of wave period are computed using an empirical function relating the mean peak wave period to the local wind speed and water depth (Young and Verhagen, 1996; Breugem and Holthuijsen, 2007; Carniello et al., 2011). The bottom shear stress induced by wind waves, τ_{ww}, is computed as a function of the maximum horizontal orbital velocity at the bottom, which is related to the significant wave height through the linear theory.
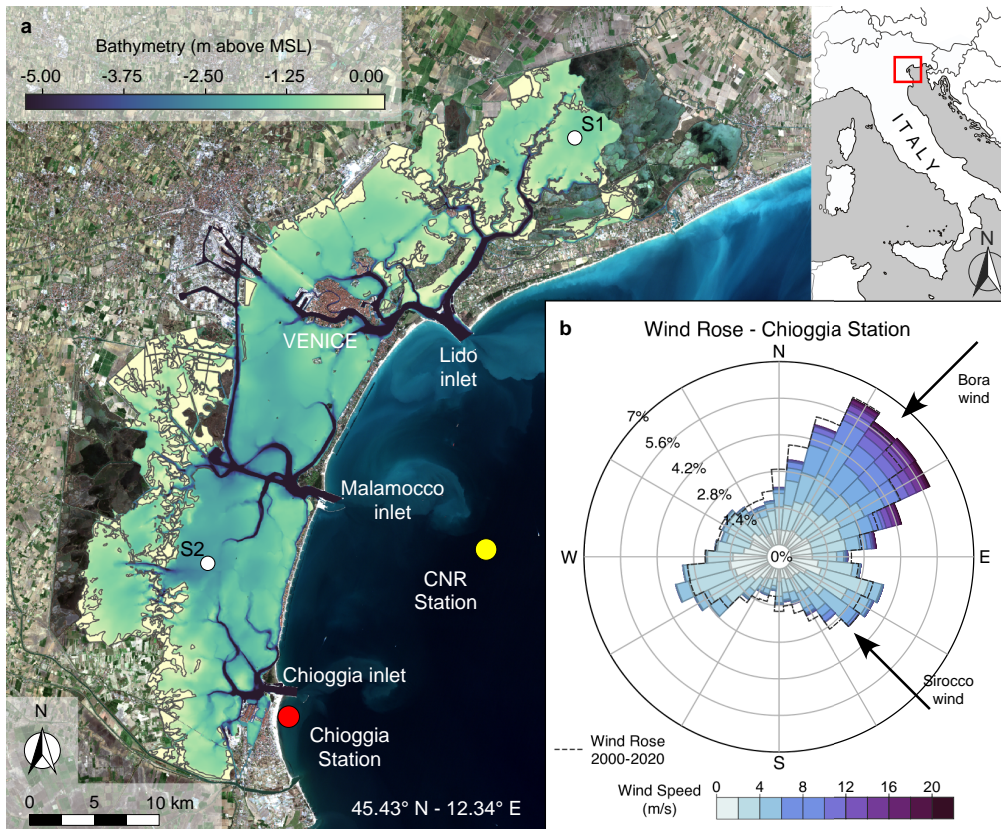
Figure 1. Morphological features and wind conditions characterizing the Venice Lagoon. a, Bathymetry of the Venice Lagoon (Base satellite image: Copernicus Sentinel data 2020, https://scihub.copernicus.eu/). The locations of the anemometric (Chioggia) and oceanographic (CNR Oceanographic Platform) stations are also shown, together with the locations of the two stations (S1 and S2) for which we provide detailed statistical characterization of over-threshold events. **b**, Wind rose for the data recorded at the Chioggia station in 2005. Dashed line shows the wind rose for the period 2000-2020.

The WWTM provides both current- and wave-induced bottom shear stresses. The bottom shear stress induced by currents, τ_{tc}, is computed using the Strickler formulation, which, in the case of a turbulent flow over a rough wall, reads (Defina, 2000)

$$\tau_{tc} = \rho g Y \left(\frac{|\boldsymbol{q}|}{K_s^2 H^{10/3}} \right) \boldsymbol{q} \tag{1}$$

where ρ is water density, g is the gravity acceleration, Y is the effective water depth (i.e. the actual volume of water per unit area), $\boldsymbol{q}$ is the flow rate per unit width, K_s is the Strickler roughness coefficient, and H is an equivalent water depth accounting for ground irregularities (Defina, 2000). The bottom shear stress induced by wind waves, τ_{ww}, is computed as a function of the total horizontal orbital velocity at the bottom, u_m, and the wave friction factor, f_w, as follows

$$\tau_{ww} = \frac{1}{2} \rho f_w u_m^2 \tag{2}$$

The bottom orbital velocity, u_m, is evaluated by applying the linear theory and is also used, together with the wave period and median grain size, to compute the wave friction factor (Soulsby, 1997). Because of the non-linear interaction between the wave and current boundary layers, the total bottom shear stress, τ_{wc}, is enhanced beyond the linear addition of the current- and wave-driven stresses. To account for this process, in the WWTM the empirical formulation suggested by Soulsby (1995, 1997) is adopted:

$$\tau_{wc} = \tau_{tc} + \tau_{ww} \left[1 + 1.2 \left(\frac{\tau_{ww}}{\tau_{ww} + \tau_{tc}} \right) \right] \tag{3}$$

The sediment transport and bed evolution module (STABEM, Carniello et al., 2012) is based on the solution of the advection-diffusion equation and Exner's equation:

$$\frac{\partial C_i Y}{\partial t} + \nabla \cdot (\boldsymbol{q} C_i) - \nabla \cdot (\boldsymbol{D_h} \nabla C_i) = E_i - D_i \qquad i = s, m \tag{4}$$

$$(1 - n) \frac{\partial z_b}{\partial t} = \sum_i (D_i - E_i) \tag{5}$$

where C is the depth-averaged sediment concentration, $\boldsymbol{D_h}(x, y, t)$ represents the space- and time-dependent 2-D diffusion tensor, E and D are the entrainment and deposition rate of bed sediment, z_b is the bed elevation and n is the bed porosity, assumed equal to 0.4. The subscript i refers to the sediment classes, that in shallow tidal environments are typically represented by non-cohesive (sand - s) and cohesive (mud - m) sediment. The relative local content of mud (p_m) can be used to mark off the transition between the cohesive or non-cohesive nature of the mixture and determines the critical value of the bottom shear stress. To discriminate between non-cohesive and cohesive behaviours, the threshold value of mud content p_{mc} is set equal to 10 % (van Ledden et al., 2004).

The deposition rate of pure sand, D_s, is given by

$$D_s = w_s r_0 C_s \tag{6}$$

where w_s is the sand settling velocity and r_0 is the ratio of near-bed to depth-averaged concentration, which is assumed constant and equal to 1.4 (Parker et al., 1987).

The deposition rate of pure cohesive mud, D_m, is computed using Krone's formula:

$$D_m = w_m C_m \max\{0; 1 - \tau_{wc}/\tau_c\} \tag{7}$$

where w_m is the mud settling velocity, τ_{wc} is the bottom shear stress, and τ_d is the critical shear stress for deposition. The settling velocities, w_s and w_m, are computed using the formulation proposed by van Rijn (1984) for solitary particles in clear and still water, thus not incorporating flocculation effects that are negligible for particle diameters larger than 20 μm (Mehta et al., 1989). The critical shear stress for deposition, τ_d, largely varies among different tidal systems and, for the Venice Lagoon, we set $\tau_d = 1$ Pa on the basis of field measurements (Amos et al., 2004).

Both sand and mud erosion rates strongly depend on the cohesive nature of the mixture. The erosion rate for pure sand, E_s, is described by the van Rijn (1984) formulation when the mixture is non-cohesive ($p_m \leq p_{mc}$) and by the Partheniades'

formula for cohesive mixtures ($p_m > p_{mc}$):

$$E_s = \begin{cases} (1-p_m)w_s \cdot 1.5 \left(\dfrac{D_{50}/Y}{D_*^{0.3}} \right) T^{1.5} & \text{for } p_m \leq p_{mc} \\[4mm] (1-p_m) \cdot M_c T & \text{for } p_m > p_{mc} \end{cases} \tag{8}$$

The erosion rate for pure mud, E_m, is described by the formulation proposed by van Ledden et al. (2004) for non-cohesive mixtures ($p_m \leq p_{mc}$) and by the Partheniades' formula for cohesive mixtures ($p_m > p_{mc}$):

$$E_m = \begin{cases} \dfrac{p_m}{1-p_m} \cdot M_{nc} T & \text{for } p_m \leq p_{mc} \\[4mm] p_m \cdot M_c T & \text{for } p_m > p_{mc} \end{cases} \tag{9}$$

In Eqs. 8 and 9, D_* denotes the dimensionless grain size and it is computed as $D_* = D_{50}[(s-1)g/\nu^2]^{1/3}$, where s is the sediment-specific density and ν is the water kinematic viscosity; T is the transport parameter; M_{nc} and M_c are the specific entrainments for non-cohesive and cohesive mixtures, respectively, which can be computed as (van Rijn, 1984; van Ledden et al., 2004):

$$M_{nc} = \alpha \frac{\sqrt{(s-1)gD_{50}}}{D_*^{0.9}}$$
$$M_c = \left(\frac{M_{nc}}{M_m} \cdot \frac{1}{1-p_{mc}} \right)^{\frac{1-p_m}{1-p_{mc}}} \cdot M_m \tag{10}$$

where M_m is the specific entrainment for pure mud and it is set equal to $5 \cdot 10^{-2}$ g m s^{-1} and the parameter α is equal to $1 \cdot 10^{-5}$ (Carniello et al., 2012).

This module uses two size classes of sediments to describe the bed composition (i.e. non-cohesive sand and cohesive mud), in order to consider the simultaneous presence of cohesive and non-cohesive sediment typically characterizing tidal lagoons (van Ledden et al., 2004). The local mud content, which varies both in space and time, marks off the transition between the cohesive and non-cohesive behaviour of a mixture, and, consequently, determines the critical value for bottom shear stress, which is locally estimated based on the critical values assumed for pure sand and pure mud. However, this task is tough and site-specific, and, moreover, field data are often limited compared to the spatial variability of bed composition. To address this issue, field surveys in the Venice Lagoon have been used to identify an empirical relationship between the local bed composition and both the local bottom elevation and the distance from the inlets. We refer to Carniello et al. (2012) for further details.

Another peculiarity of the sediment transport module is the stochastic approach chosen to model the near-threshold conditions for sediment entrainment. Indeed, in shallow tidal basins, resuspension events are periodically driven by bottom shear stresses that slightly exceed the erosion threshold. The bottom shear stress, as well as the critical shear stress, is very unsteady owing to the non-uniform flow velocity, wave characteristics and small-scale bottom heterogeneity.

The transport parameter, T, is usually defined as $T = \max\{0; \tau_{wc}/\tau_c - 1\}$ where τ_c is the critical shear stress for erosion and can be assumed to vary monotonically between the critical value for pure sand, τ_{cs}, and the critical value for pure mud,

τ_{cm}, depending on the mud content (van Ledden et al., 2004):

$$\tau_c = \begin{cases} (1+p_m)\tau_{cs} & \text{for } p_m \leq p_{mc} \\ \dfrac{\tau_{cs}(1+p_{mc}) - \tau_{cm}}{1 - p_{mc}}(1-p_m) + \tau_{cm} & \text{for } p_m > p_{mc} \end{cases} \tag{11}$$

However, this classic definition of the transport parameter describes a sharp transition between $T = 0$ and $T = \tau_{wc}/\tau_c - 1$ that does not take into account the spatial and temporal variability of both τ_{wc} and τ_c. Indeed, in real tidal systems, the bottom shear stress slightly varies owing to the non-uniform flow velocity, wave characteristics and small-scale bottom heterogeneity, while the critical shear stress is also affected by the random grain exposure and bed composition in time and space. Hence, following the stochastic approach suggested by Grass (1970), both the total bottom shear stress, τ_{wc}, and the critical shear stress for erosion, τ_c, are treated as random variables (τ_{wc}', and τ_c', respectively) with lognormal distributions, and their expected values are those calculated by WWTM and STABEM. Consequently, the erosion rate depends on the probability that τ_{wc}' exceeds τ_c' (Carniello et al., 2012). The result of this stochastic approach is a smooth transition between $T = 0$ and $T = \tau_{wc}/\tau_c - 1$. The comparison with SSC field measurements shows a much better agreement of the stochastic approach compared to that of the classic formulation (Supplementary information and Figure S3). Finally, erosion and deposition rates of sand and mud result in a variation of bed level and composition through time, which is computed using Eq. 5 and updating the local mud content.

The model has been widely calibrated and tested in the most recent configuration of the Venice Lagoon, i.e., when field data are available. Since the hydrodynamic model performance has been reported when considering the erosion dynamics (D'Alpaos et al., 2023), here we summarize the ability of the sediment transport model to reproduce SSC by reporting the standard Nash-Sutcliffe Model Efficiency (NSE) parameter computed when field data are available and refer the interested reader to the Supplementary Information (Figures S4 and S5) and the literature (Carniello et al., 2012; Tognin et al., 2022) for a more detailed comparison. Adopting the classification proposed by Allen et al. (2007), the model performance can be rated from excellent to poor (i.e., NSE > 0.65 excellent; 0.5 < NSE < 0.65 very good; 0.2 < NSE < 0.5 good; NSE < 0.2 poor). The STABEM model is very good to excellent in reproducing SSC ($NSE_{mean} = 0.65$, $NSE_{median} = 0.62$, $NSE_{std} = 0.17$, statistics are derived from calibration reported in Carniello et al. (2012), their Tables 2 and 3, and Tognin et al. (2022), their Table S2). Importantly, the sediment transport model not only correctly reproduces the magnitude of the SSC but also captures its modulation induced by tidal currents and wind-wave variations (Figures S4 and S5).

The coupled hydrodynamic and sediment transport ~~These coupled numerical~~ models were used to perform one-year-long simulations within the six different computational grids representing the historical configurations of the Venice Lagoon and the portion of the Adriatic Sea in front of it. Hourly tidal level gauged at the Consiglio Nazionale delle Ricerche (CNR) Oceanographic Platform, located in the Adriatic Sea offshore of the lagoon, and wind velocities and directions recorded at the Chioggia anemometric station are imposed as boundary conditions (Figure 1).

All configurations were forced with tidal levels and wind climate measured during the whole year 2005, because the cumulative distribution frequency of wind velocity measured in 2005 is the closest to that of the whole period 2000-2020 (D'Alpaos et al., 2023), and, consequently, can be considered a representative year for the wind climate (Figure 1). ~~as this~~

 Forcing all the historical configurations of the Venice Lagoon with the same wind and tidal conditions enables us to isolate the effects of the morphological modifications on the wind-wave field, hydrodynamics and sediment dynamics. Because bed elevation in each computational grid refers to the mean sea level at the time of each survey, we implicitly take into account the effects of historical relative sea level variations.

To correctly model SSC as well as bed evolution, the knowledge of the bed sediment composition is crucial. Sufficiently detailed, spatially-distributed grain-size data are available for the present-day configuration of the Venice Lagoon (Amos et al., 2004; Umgiesser et al., 2006). Using this dataset, Carniello et al. (2012) empirically related the median grain size D_{50} to the local bottom elevation and the distance from the inlets:

$$D_{hf} = \begin{cases} \max\{300; 50(-h_f - 0.8)^{0.75}\} & \text{if } h_f \leq 1 \text{ m a.m.s.l.} \\ 15 & \text{if } h_f > 1 \text{ m a.m.s.l.} \end{cases} \tag{12}$$

$$D_{50} = D_{hf} + 100e^{-0.0097L^3} \tag{13}$$

where h_f is the bottom elevation in m a.m.s.l.; L is the linear distance from the closer inlet in km; D_{50} and D_{hf} are the grain diameter μm. This relationship describes a coarsening of the sediment grain size distribution at deeper locations (i.e. channels) and at shorter distances from the sea (Figure S2). Because bottom elevation and the distance from the inlet are the two main parameters describing the spatial variation in sediment grain size, we assume that this relationship holds independently on the specific morphological configuration of the Venice Lagoon and we used Eqs. 12 and 13 to compute the distribution of median grain size D_{50} in all the six selected historical configurations.

The spatial distribution of mud content, p_m, is then computed as a combination of the local D_{50} and the typical grain size of mud and sand fractions (Umgiesser et al., 2006)

$$p_m = 1 - \frac{\ln(D_{50}/D_m)}{\ln(D_s/D_m)} \tag{14}$$

where D_m and D_s are the typical grain size of mud and sand, respectively. Analysing the grain size distribution measured in the Venice Lagoon (Amos et al., 2004; Umgiesser et al., 2006), we set $D_m = 20\ \mu$m and $D_s = 200\ \mu$m.

Another important issue to consider when studying SSC dynamics in shallow tidal environments is the presence of benthic and halophytic vegetation, which both shelters the bed against the hydrodynamic action and increases the local critical shear stress for erosion because of the presence of roots. While the presence of halophytic vegetation over salt marshes is almost ubiquitous, reconstructing the presence of benthic vegetation on the tidal flats is much more difficult even for the present configuration of the lagoon and practically impossible for the ancient configurations (Goodwin et al., 2023). For the above reasons and for the sake of homogeneity, the simulations of the present study neglect the presence of benthic vegetation on the tidal flat and assume all salt-marsh platforms to be completely vegetated in each configuration of the lagoon, thus neglecting sediment resuspension over them (Christiansen et al., 2000; Temmerman et al., 2005).

2.2 Peak Over Threshold Analysis of SSC

Sediment transport dynamics in tidal environments are the results of the complex interplay among hydrodynamic, biologic, and geomorphologic processes. This interplay between different factors can be fully framed only by taking into account both its deterministic and stochastic components. As an example, Carniello et al. (2011) argued that morphological dynamics in the Venice Lagoon are mostly linked to a few severe resuspension events induced by wind waves, whose dynamics are markedly stochastic in the present configuration (D'Alpaos et al., 2013; Carniello et al., 2016). Measurements confirm that high SSC events are also important sediment suppliers for salt marshes (Tognin et al., 2021).

In the present work, we used the peak-over-threshold theory (POT) (Balkema and de Haan, 1974) to analyze temporal and spatial dynamics of the total SSC at any location within each selected configuration of the Venice lagoon.

First, a minimum-intensity threshold, C_0, was chosen to identify the set of over-threshold events from the modelled SSC record, and then a statistical analysis of interarrival times, durations and intensities of the exceedances of the threshold was carried out.

The interplay among the different drivers that control suspended sediment dynamics in shallow tidal environments can be fully framed only by taking into account also its stochastic components, associated with wind waves and storm surges, which are largely responsible for the morphodynamic evolution of these systems (Carniello et al., 2011; Tognin et al., 2021). To this aim, in the present work, we statistically characterize the spatial and temporal dynamics of resuspension events by applying the peak-over-threshold theory (POT) (Balkema and de Haan, 1974) to the one-year-long time series of SSC computed with the numerical model described above for the different configurations of the Venice Lagoon.

Before applying the POT analysis, the SSC time series provided by the numerical simulations were low-pass filtered by applying a moving average procedure with a time window of 6 hours, in order to preserve the tide-induced modulation of the signal but, at the same time, to remove artificial upcrossing and downcrossing of the threshold, generated by short-term fluctuations. This pre-processing procedure prevents the identification of a false dependence of subsequent over-threshold events due to spurious fluctuations.

Once a proper threshold, C_0, is chosen, the POT identifies three different random variables: interarrival times, durations and intensities of the exceedances of the threshold. The interarrival time is defined as the time interval between two consecutive upcrossings of the threshold, the duration of the events is the time elapsed between any upcrossing and the subsequent downcrossing of the threshold, and, finally, the intensity is calculated as the largest exceedance of the threshold in the time-lapse between an upcrossing and the subsequent downcrossing. These random variables are characterized by their probability density functions and the corresponding moments for any location in all the considered configurations of the Venice Lagoon, in order to provide a complete description of the SSC pattern. Besides synthetically characterising over-threshold events, these three variables can be combined to compute more complex metrics to describe SSC dynamics (e.g. the volume of sediment reworked in a selected time frame).

The nature of the stochastic processes can be determined by the analysis of the interarrival times distribution. Indeed, resuspension events can be mathematically modelled as a Poisson process if the interarrival times between subsequent exceedances

of the threshold, C_0, are independent and exponentially distributed random variables (Cramér and Leadbetter, 1967; Gallager, 2013). Moreover, the memorylessness of the Poisson process guarantees that the number of events observed in disjoint sub-periods is an independent, Poisson-distributed random variable (Gallager, 2013). When the sequence of random events that define a 1-D Poisson process along the time axis can be associated with a vector of random marks that defines the duration and intensity of each over-threshold event, the process can be defined as a marked Poisson process. The distribution of these marks does not affect the chance to model the process as Poissonian, which, indeed, relies only on the exponentiality of interarrival times. However, when also duration and intensity are exponentially distributed, the set-up of a stochastic framework can be further simplified. In order to assess that over-threshold SSC events can be modelled as a marked Poisson process, we performed the Kolmogorov-Smirnov (KS) goodness of fit test on the distribution of the interarrival times, intensity and duration of over-threshold events.

In the POT analysis, the threshold value plays a critical role and its choice deserves careful attention. In the case of erosion dynamics (D'Alpaos et al., 2023), the identification of the threshold with the critical shear stress for erosion seems to be quite straightforward and has the advantage of preserving also the physical meaning of the process. Instead, when dealing with SSC, the absence of a clear physical threshold mechanism may make the identification of the threshold value less direct. The present analysis aims to characterize the bulk effect of morphologically meaningful SSC events, rather than to describe only the extreme events, and, simultaneously, to remove the weak resuspension events induced by periodic tidal currents that can be described as a recurrent, deterministic process. From this point of view, the choice of a threshold value, C_0, that identifies morphologically significant over-threshold SSC events, has to consider two opposite requirements. On the one hand, stochastic sediment concentration generated by storm-induced wind waves can be distinguished from tide-modulated daily concentration only if C_0 is large enough. On the other hand, too high values of C_0 either require a long, computationally prohibitive simulated time series or can lead to a non-informative analysis because of the large number of events unaccounted for. These observations narrow the range in which the threshold can be selected. The lower boundary is set by the SSC observed in the absence of wind and, therefore, associated exclusively with the tide. While the upper boundary has to be maintained well below the maximum observed values to consider all the morphologically meaningful events. In the specific case of the Venice Lagoon, to satisfy these requirements, the C_0 value has to fall between 30 and 60 mg l^{-1}, as suggested by in-situ SSC measurements (Carniello et al., 2012, 2014).

The sensitivity analysis performed on the present-day configuration of the Venice Lagoon (Carniello et al., 2016) suggests that the chance to model SSC events as a Poisson process is weakly affected by the specific threshold value in the above range. Indeed, using threshold values equal to 30, 40, 50 or 60 mg l^{-1} hardly changes the areas where interarrival times are not exponentially distributed and, therefore, wind-induced SSC cannot be described as a Poisson process (Figure S6). On the basis of these observations and to allow the comparison among the different configurations, in the present analysis, we used a constant threshold, C_0, equal to 40 mg l^{-1}.

According to the extreme value theory, a Poisson process emerges from a stochastic signal whenever enough high censoring threshold is chosen (Cramér and Leadbetter, 1967). However, as this present analysis is designed to remove only the weak resuspension events induced by periodic tidal currents, the critical threshold is well below the maximum observed values.

3 Results and Discussion

We analyzed the time series of computed total SSC at any node of the computational grids reproducing the six selected configurations of the Venice Lagoon on the basis of the POT method, in order to characterize the over-threshold events in terms of interarrival times, peak excess and duration. We then performed the KS test (significance level $\alpha = 0.05$) to compare the distributions of interarrival times with an exponential distribution, to test the hypothesis to model SSC events as a Poisson process. The KS test is also applied to peak excess and duration of the over-threshold events to test if these marks can be described by exponential distributions as well. The chance to model SSC dynamics as a Poisson process relies only on the exponentiality of interarrival times and it is not affected by the specific distribution of peak excess and duration. However, the set up of the final stochastic framework is simplified when also the duration and peak excess follows an exponential distribution.

Therefore, in the spatial distribution of the KS test results (Figure 2), we can identify three different situations:

1. SSC events cannot be described as a Poisson process, i.e. the KS test is not satisfied for interarrival times, in the dark blue areas;

2. SSC events are indeed a marked Poisson process because interarrival times, peak excesses and durations satisfy the KS test, and, thus, are exponentially distributed random variables, in the red areas;

3. SSC events still are a marked Poisson process but at least one between intensity and duration does not satisfy the KS test, i.e. although interarrival times follow an exponential distribution, at least one between intensity and duration does not, in the yellow areas.

The spatial distribution of mean interarrival times (Figure 3), mean intensities of peak excesses (Figure 4), and mean durations (Figure 5) of over-threshold events are shown at any location within each of the six historical configurations where SSC events can be modelled as a Poisson process (i.e., the KS test is verified for interarrival times at significance level $\alpha = 0.05$). The mean values of these three random variables are shown where at least interarrival times are exponentially distributed (i.e. yellow areas in Figure 2) because the SSC dynamics can be modelled as a Poisson process although the marks are described by a distribution different from the exponential one and mean peak excess and mean duration are nonetheless informative.

The area of the lagoon where over-thresholds SSC events cannot be modelled as Poisson processes are mostly represented by salt marshes and tidal channels in all configurations (see dark blue areas in Figure 2), similarly to the results for bottom shear stresserosion events (BSS) (D'Alpaos et al., 2023). On salt-marsh areas, both BSS and SSC thresholds (τ_C and C_0 respectively) are seldom exceeded (Figure S7 and S8), because the reduced water depth over the marsh prevents the propagation of large wind waves and the presence of halophytic vegetation limits sediment advection by promoting deposition and stabilizes the bottom preventing erosion (e.g., Möller et al., 1999; Temmerman et al., 2005; Carniello et al., 2005). Within the main tidal channels and at the three inlets, as happens for BSS, SSC dynamics are not Poissonian, but the reason why interarrival times of erosion and SSC events are not exponentially distributed are slightly different. In the main channel network and at the inlets, SSC exceeds the threshold value, C_0, very few times or it does not exceed the threshold at all, due to vertical dispersion mechanisms that decrease the local concentration of sediment in suspension in deeper areas (Figure S8). Conversely, BSS typically exceeds the threshold τ_c twice or four times a day (Figure S7) mainly because of the tide action but the BSS time evolution cannot be modelled as a Poisson process as confirmed by the KS test on interarrival times of over-threshold BSS events (D'Alpaos et al., 2023).

However, SSC events can be modelled as a Poisson process over wide areas of the six configurations of the Venice Lagoon, in particular over tidal flats and subtidal platforms (see red and yellow areas in Figure 2). As a consequence, SSC dynamics can be effectively modelled by using a synthetic framework based on Poisson processes over widespread portions of the different morphological configurations experienced by the Venice Lagoon in the last four centuries.

Large interarrival times (i.e., larger than 30 days, Figure 3) are observed on tidal flats close to the main channel network because dilution processes within higher water depth, enhanced by the higher velocities in these sites, reduce sediment concentration, and hence only severe, but infrequent, events can lead to an exceedance of the threshold. Sheltered areas are also characterized by large interarrival times as represented by the northern portion of the lagoon, which is protected by the main-
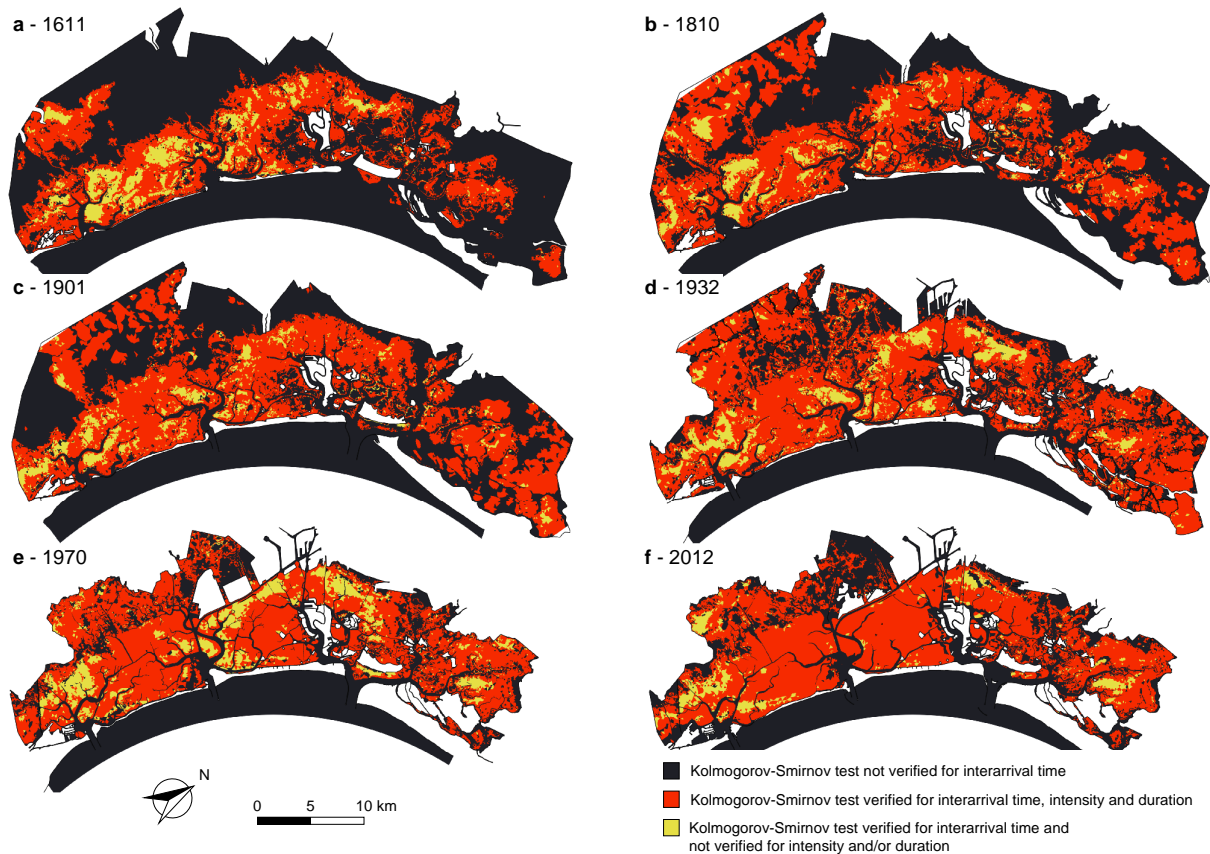
Figure 2. Kolmogorov-Smirnov test for over-threshold SSC events. Spatial distribution of Kolmogorov-Smirnov (KS) test at significance level ($\alpha = 0.05$) for the six different configurations of the Venice Lagoon: (a) 1611, (b) 1810, (c) 1901, (d) 1932, (e) 1970, and (f) 2012. ~~1611 (a), 1810 (b), 1901 (c), 1932 (d), 1970 (e), and 2012 (f).~~ In the maps we can distinguish areas where the KS test is: not verified (dark blue); verified for all the considered stochastic variables (interarrival time, intensity over the threshold and duration) (red); verified for the interarrival time and not for intensity and/or duration (yellow).

land from the north-easterly Bora wind, which is the most intense and morphologically significant wind in the Venice Lagoon (Figure 1b), and where the presence of extensive salt-marsh areas continuously interrupts the propagation of wind waves. In this case, the reduced number of upcrossing events, and, consequently, large interarrival times is due to the sheltering action of salt marshes and islands in reducing wind-wave resuspension. SSC events over the marsh platform slightly changed through centuries. In the three oldest configurations (i.e., 1611, 1810 and 1901) mainly because of the wide extent of salt marshes, resuspension events over salt marshes do not even reach the threshold, as shown by the number of upcrossing (Figure S8). In the more recent ones, where salt-marsh extent importantly decreases, marshes start experiencing some over-threshold SSC events because of the advection of sediment from the adjacent areas, but the lower number of upcrossing allows the mean interarrival time to assume large values.
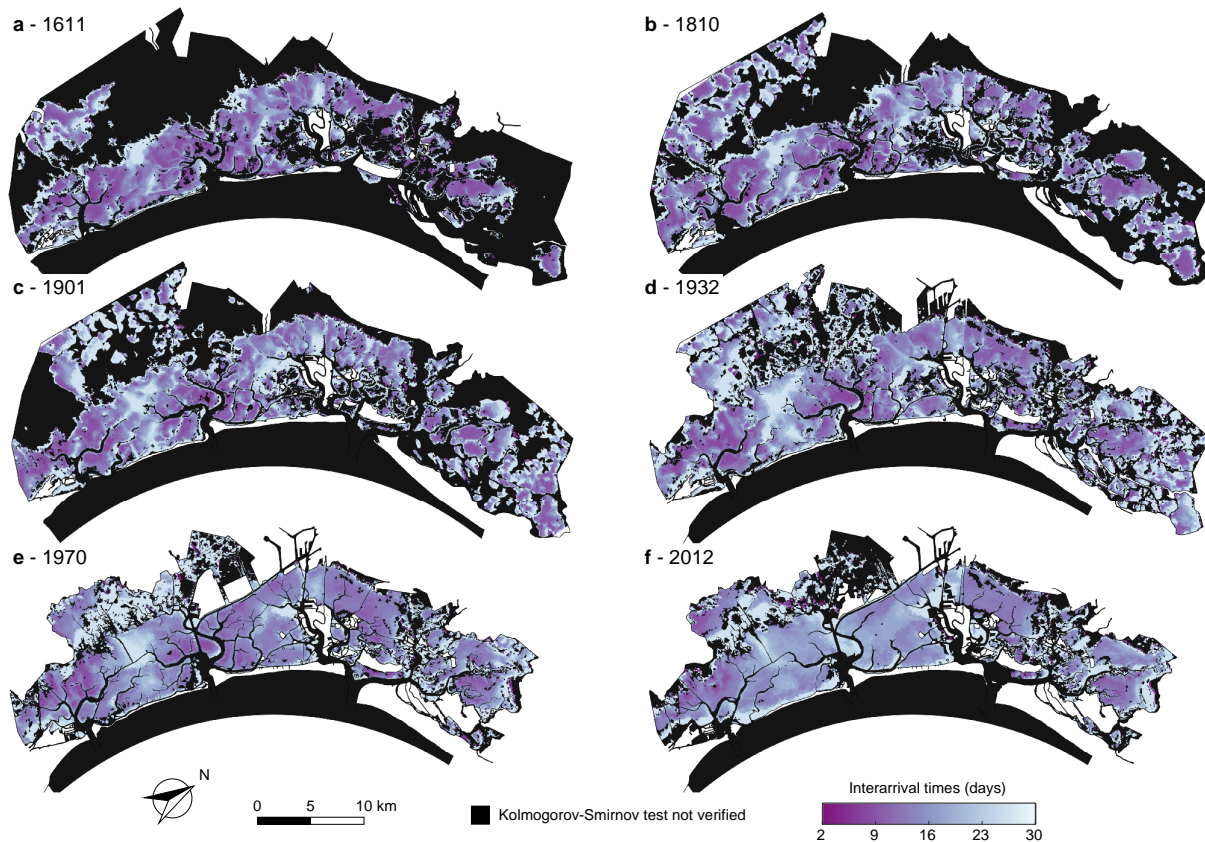
Figure 3. Mean interarrival time of over-threshold SSC events. Spatial distribution of mean interarrival times of over-threshold exceedances at sites where SSC events can be modelled as a marked Poisson process, as confirmed by the KS test ($\alpha = 0.05$) for the six different configurations of the Venice Lagoon: (**a**) 1611, (**b**) 1810, (**c**) 1901, (**d**) 1932, (**e**) 1970, and (**f**) 2012. ~~1611 (**a**), 1810 (**b**), 1901 (**c**), 1932 (**d**), 1970 (**e**), and 2012 (**f**).~~

Over wide tidal flat areas, where the threshold is exceeded in all the considered configurations, the mean interarrival time generally slightly increases through the centuries (Figure S10a). This trend is more evident in the central and southern parts of the lagoon, where, because of the deepening experienced in the last century, the number of events able to resuspend sediments

470 from the bottom decreased importantly, hence increasing the mean interarrival time of intense SSC events. In fact, over the central-southern shallow tidal flats of the four most ancient configurations, interarrival times present relatively low values (about 10 days), whereas they generally become longer (between 20 and 25 days) in the same areas in the more recent configurations. On the contrary, in the better preserved, northern portion of the lagoon, where the fetch is continuously interrupted by islands, spits, and salt marshes also in the more recent configurations, the mean interarrival times experienced only slight changes

475 over centuries. As an example, Figure 6a shows the mean interarrival times, λ_t, experienced by the "Palude Maggiore" tidal flat (station S1 in Figure 1) that do not vary remarkably over time. On the contrary, the subtidal flat at the watershed divide
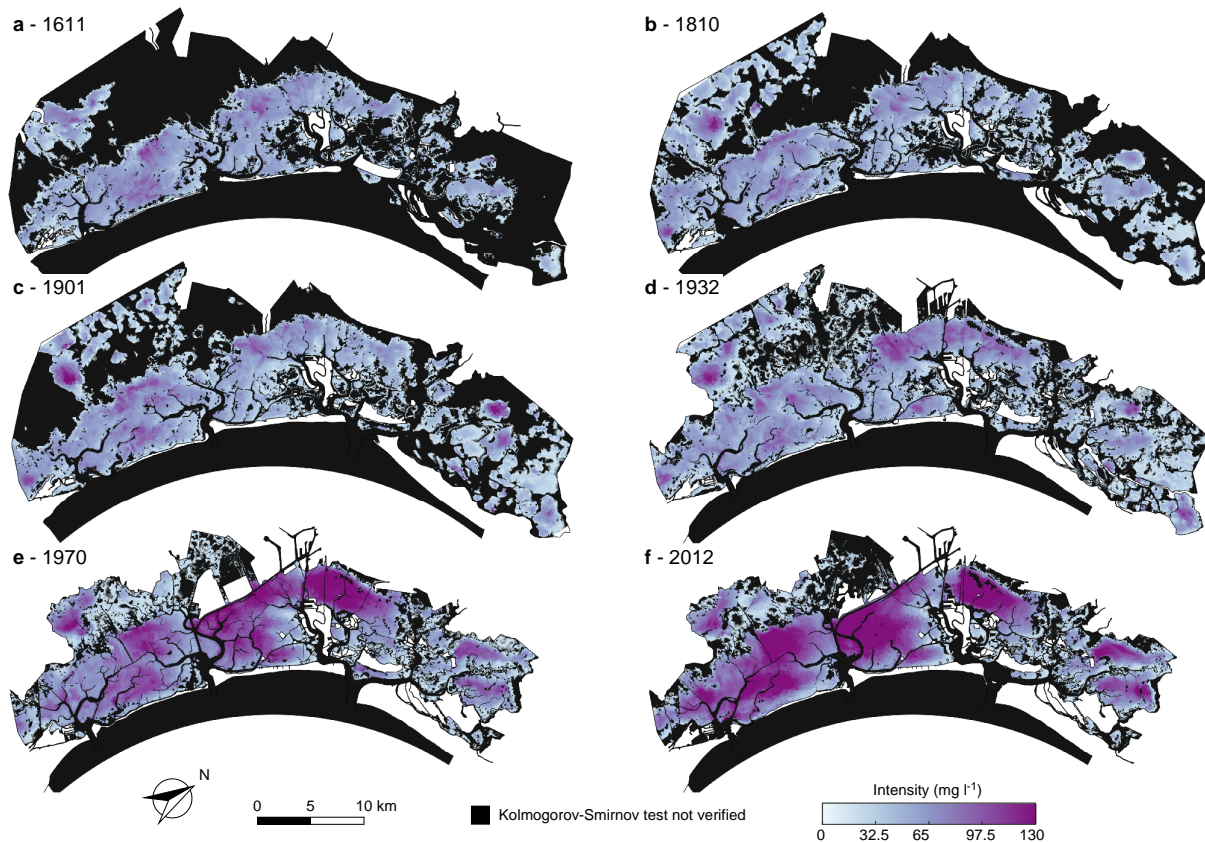
Figure 4. Mean intensity of over-threshold SSC events. Spatial distribution of mean intensity of peak excesses of over-threshold exceedances at sites where SSC events can be modelled as a marked Poisson process, as confirmed by the KS test ($\alpha = 0.05$) for the six different configurations of the Venice Lagoon: (**a**) 1611, (**b**) 1810, (**c**) 1901, (**d**) 1932, (**e**) 1970, and (**f**) 2012. ~~1611 (**a**), 1810 (**b**), 1901 (**c**), 1932 (**d**), 1970 (**e**), and 2012 (**f**).~~

between the Chioggia and Malamocco inlets, known as "Fondo dei Sette Morti" (station S2 in Figure 1), display a much larger variation of λ_t with decreasing interarrival times through centuries (Figure 6d). In the more ancient configurations, thanks to its relatively lower depth and its position sheltered by shallower tidal flats, station S2 experienced over-threshold events only during severe events. In the more recent configurations, over-threshold events become more frequent due to the deepening of the surrounding tidal flats, thus allowing larger waves and currents to propagate in this area and enhancing resuspension as well as suspended sediment transport.

The intensity of over-threshold events abruptly increases between 1932 and 1970 (Figure 4 and S10b). Indeed, SSC exceedance intensity maintains low mean values, generally below 60 mg l^{-1}, in all the configurations until 1932, thereafter it doubles on wide tidal-flat areas, especially in the central-southern lagoon and northwest of the city of Venice, where the action
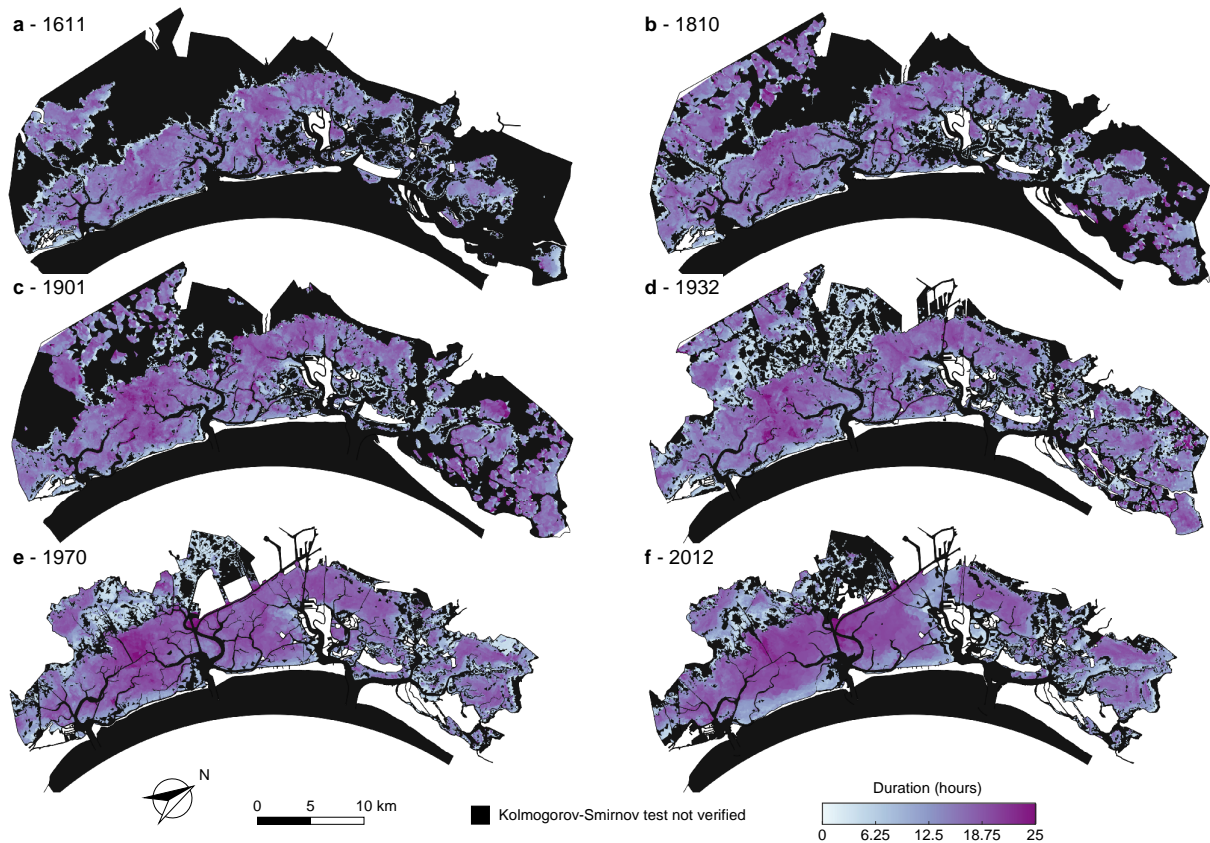
Figure 5. Mean durations of over-threshold SSC events. Spatial distribution of mean durations of over-threshold exceedances at sites where SSC events can be modelled as a marked Poisson process, as confirmed by the KS test ($\alpha = 0.05$) for the six different configurations of the Venice Lagoon: (**a**) 1611, (**b**) 1810, (**c**) 1901, (**d**) 1932, (**e**) 1970, and (**f**) 2012. ~~1611 (**a**), 1810 (**b**), 1901 (**c**), 1932 (**d**), 1970 (**e**), and 2012 (**f**).~~

of wind waves is stronger because of the generalized deepening of those areas. This analysis confirms that the intensity increase is much more important in the central lagoon (station S2, Figure 6e) than in the northern part (station S1, Figure 6b).

Overall, over-threshold event durations slightly increase through the centuries (Figure 5 and S10c). However, two different trends can be distinguished in different portions of the lagoon, likewise interarrival times and intensities. The duration increase in the more pristine, northern portion of the basin is much lower than that in the central and southern lagoon due to the heavier morphological modifications the latter areas experienced (Figure 6c and f).

SSC dynamics are affected by local entrainment and advection/dispersion processes from and toward the surrounding areas. Furthermore, the local resuspension is highly influenced by the combined effect of tidal currents and wind waves, thus depending on current velocity, water depth, fetch, wind intensity and duration (Fagherazzi and Wiberg, 2009; Carniello et al., 2016).
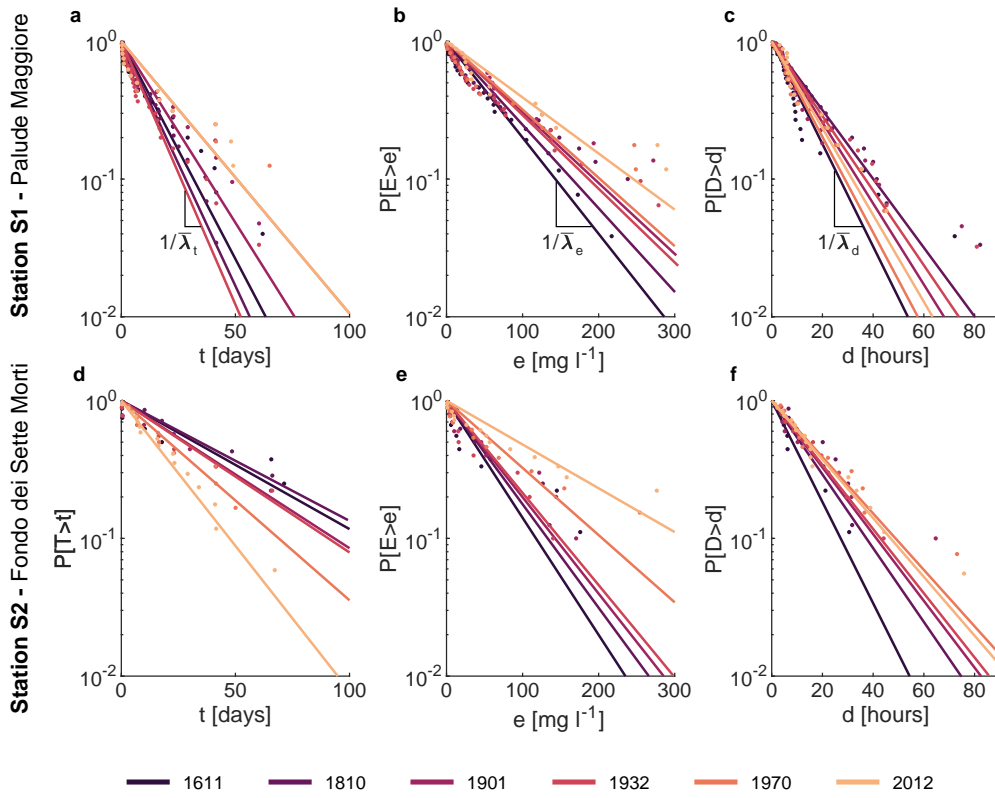
Figure 6. Over-threshold SSC events at stations S1 and S2. Statistical characterizations of over-threshold events at two stations S1 "Palude Maggiore" and S2 "Fondo dei Sette Morti" (see Figure 1a for locations) in the six configurations of the Venice Lagoon. Probability distributions of (**a-b**) interarrival times, t; (**c-d**) intensities of peak excesses of over-threshold exceedances, e; and (**e-f**) durations of over-threshold event, d. $\overline{\lambda}_t$ mean interarrival time, $\overline{\lambda}_e$ mean peak excess intensity, and $\overline{\lambda}_d$ mean duration.

495   As a consequence, the mean values of the random variables characterizing SSC events present highly heterogeneous spatial patterns in the more ancient configurations of the Venice Lagoon due to their higher morphological complexity.

    To describe the relationship between interarrival times, durations and intensities, the temporal cross-correlation between these three random variables was computed for each point within the six configurations of the Venice Lagoon (Figure S11, S12, S13). Duration of over-threshold exceedances and intensity of peak excesses are highly correlated in all the six considered

500   configurations, suggesting that longer events are linked to more intense ones (Figure S11 and S14a). On the contrary, durations and interarrival times, as well as intensities and interarrival times display almost no correlation (Figure S11, S12 and S14b,c). These relations between interarrival time, intensity and duration back up the idea that, as for BSS dynamics (D'Alpaos et al., 2023), over-threshold SSC events can be modelled as a 3-D Poisson process in which the marks (intensity and duration of over-threshold events) are mutually dependent but independent on interarrival times.

505 As a result of the cause-effect relationship between the BSS (cause) and SSC (effect), their spatial and temporal dynamics show a high cross-correlation between interarrival times (Figure 7), intensity (Figure 8) and duration (Figure 9) of BSS and SSC over-threshold events. Recalling the absence of correlation between interarrival times and both intensities and durations for both BSS and SSC events, we can conclude that, when generating synthetic time series, interarrival times of BSS and SSC events are mutually dependent but not related to their intensity and duration. Intensities and durations of SSC are instead
510 strongly correlated with the corresponding properties of BSS events.

Despite showing high similarity and correlation, BSS and SSC events are not identical. The BSS ultimately depends on the local hydrodynamics, i.e. the local value of the bed shear stress τ_{wc} produced by tidal currents and wind waves. On the contrary, the SSC is not only a function of the local entrainment but also of the suspended sediment flux from and towards the surrounding areas. As a result of the advection/dispersion processes, the spatial pattern of SSC is smoother than that of BSS.
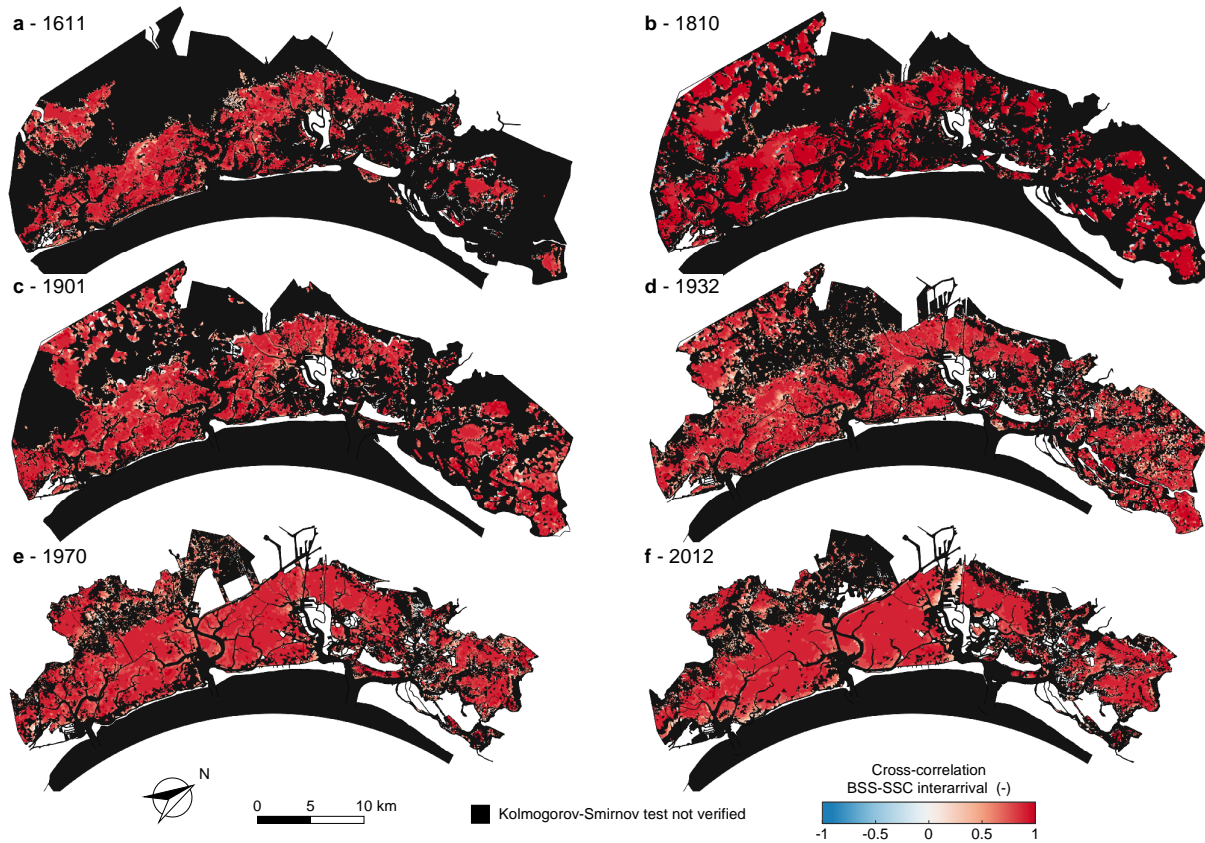
Figure 7. Cross-correlation between interarrival times of over-threshold BSS and SSC events. Spatial distribution of the cross-correlation between interarrival times of over-threshold BSS and SSC exceedances for the six different configurations of the Venice Lagoon: (a) 1611, (b) 1810, (c) 1901, (d) 1932, (e) 1970, and (f) 2012. ~~1611 (a), 1810 (b), 1901 (c), 1932 (d), 1970 (e), and 2012 (f).~~ Black identifies sites where over-threshold BSS or SSC events cannot be modelled as a marked Poisson process (i.e. the KS test is not verified for the interarrival time).
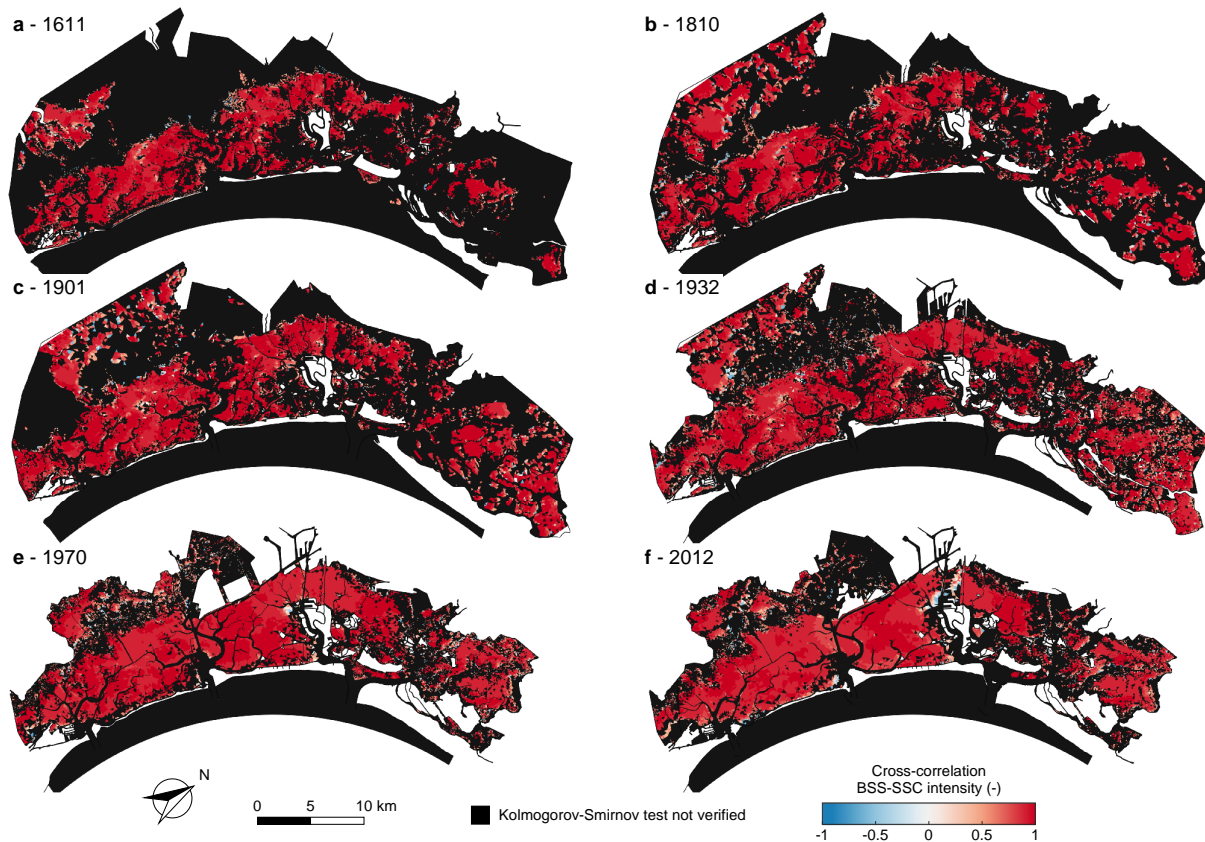
Figure 8. Cross-correlation between intensities of over-threshold BSS and SSC events. Spatial distribution of the cross-correlation between intensities of over-threshold exceedances BSS and SSC for the six different configurations of the Venice Lagoon: (a) 1611, (b) 1810, (c) 1901, (d) 1932, (e) 1970, and (f) 2012. ~~1611 (a), 1810 (b), 1901 (c), 1932 (d), 1970 (e), and 2012 (f).~~ Black identifies sites where over-threshold BSS or SSC events cannot be modelled as a marked Poisson process (i.e. the KS test is not verified for the interarrival time).

515   The statistical characterization of over-threshold SSC events using their mean interarrival times, intensities and durations can be useful to estimate the total amount of reworked sediments. Although different portions of the lagoon experience different trends in these parameters depending on specific morphological modifications, a spatial average over the whole area where over-threshold SSC events can be described as Poisson processes shows that globally mean interarrival times and duration slightly vary and remain almost equal to about 30 days and 13 hours, respectively (Figure S10a and c). By contrast, intensity of

520   the peak excess abruptly changes between 1932 and 1970. Between 1611 and 1932 the mean intensity maintains a value lower than 45 mg l^{-1}, but increases to 64 mg l^{-1} in 1970 and further to 73 mg l^{-1} in 2012 (Figure S10b).

This increase in the intensity of over-threshold SSC events, which is clearly associated with the generalized deepening of the tidal-flat areas, generates an increase in the amount of reworked sediment. This means that on average every month, for about 13 hours, the amount of sediment mobilized within the basin increases from about $2 \cdot 10^6$ kg in the three most
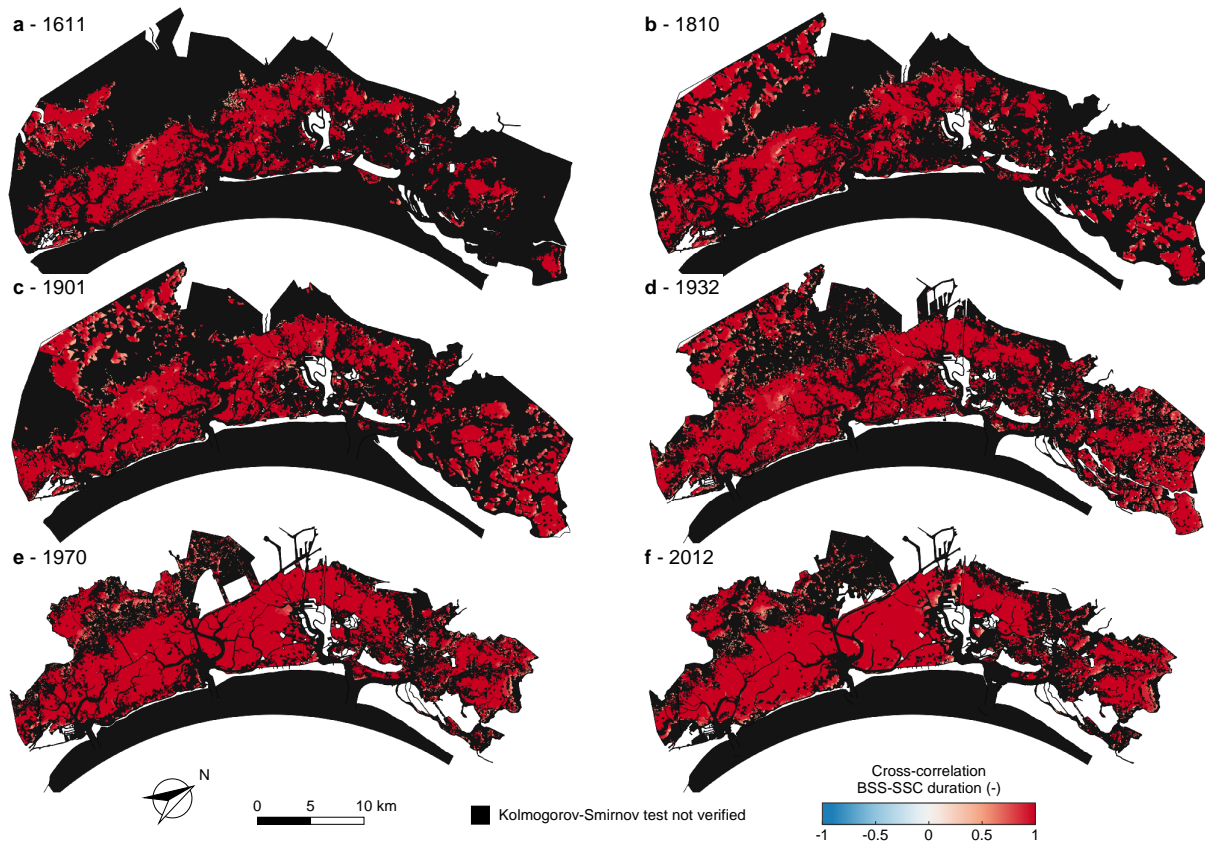
Figure 9. Cross-correlation between durations of over-threshold BSS and SSC events. Spatial distribution of the cross-correlation between durations of over-threshold exceedances BSS and SSC for the six different configurations of the Venice Lagoon: (**a**) 1611, (**b**) 1810, (**c**) 1901, (**d**) 1932, (**e**) 1970, and (**f**) 2012. ~~1611 (**a**), 1810 (**b**), 1901 (**c**), 1932 (**d**), 1970 (**e**), and 2012 (**f**).~~ Black identifies sites where over-threshold BSS or SSC events cannot be modelled as a marked Poisson process (i.e. the KS test is not verified for the interarrival time).

ancient configurations to more than $6.8 \cdot 10^6$ kg in the 2012 configuration (Table 1). Besides directly boosting the amount of sediment available for export toward the open sea given the ebb-dominated character of the Venice Lagoon (Ferrarin et al., 2015; Finotello et al., 2023), the increase of suspended sediment also affects numerous biological and ecological processes that in turn influence the morphological evolution of the tidal system (e.g., Venier et al., 2014; Pivato et al., 2019).

As already mentioned, modelling the morphodynamic evolution of tidal landscapes over long timescales (decades or centuries) necessarily requires the use of simplified approaches. However, a classical assumption of long-term evolution models is that the sediment supply is constant or monotonically related to mean water depth. The results presented in this study, together with those obtained for erosion events (D'Alpaos et al., 2023), demonstrate that the time series of both BSS and SSC can be described as marked Poisson processes with exponentially distributed interarrival times, intensities, and durations, thereby setting a framework for the synthetic generation of statistically significant external forcing factors (shear stress at the bottom

Table 1. Sediment reworking in the historical configurations of the Venice Lagoon. *area* (km^2): area of the lagoon where KS is verified; h (m): mean water depth of the area; V_w (10^6 m^3): mean volume of water, obtained as product of area and water depth; e (mg l^{-1}): mean intensity of over-threshold SSC events; S_{mob} (10^6 kg): sediment mobilized, assuming a triangular-shaped temporal evolution of over-threshold SSC events, with peak excess e.

Year	area (km^2)	h (m)	V_w (10^6 m^3)	e (mg l^{-1})	S_{mob} (10^6 kg)
1611	226.882	0.59	134.403	44.20	1.980
1810	294.649	0.43	127.022	40.84	1.729
1901	307.951	0.47	143.985	42.66	2.047
1932	350.166	0.54	188.661	43.49	2.734
1970	283.196	0.77	217.863	64.16	4.659
2012	270.022	1.04	279.969	73.21	6.832

and suspended sediment available in the water column) that should improve the reliability of long-term biomorphodynamic models with a limited increase in the number of parameters.

4   Conclusions

SSC dynamics in shallow tidal environments is usually investigated by means of field measurements or remote sensing analysis. However, due to the limited spatial coverage of field measurement and the temporal resolution of satellite images, long-term SSC dynamics at the basin scale are seldom available. Numerical models, once properly calibrated and tested, can provide reliable long SSC time series which can be used to statistically characterize the spatial and temporal variability of intense SSC events.

In the present study, we applied a custom-built, extensively tested, 2-D finite-element numerical model to reproduce SSC dynamics at basin scale in six historical configurations of the Venice Lagoon, covering a time span of four centuries. The computed SSC time series were analysed on the basis of the peak-over-threshold theory. Statistical analyses suggest that over-threshold SSC events can be modelled as a marked Poisson process over wide areas of all the selected configurations of the Venice Lagoon.

We found that, due to the morphological evolution experienced by the lagoon in the last four centuries, mean interarrival time, intensity and duration of over-threshold events generally increase through the centuries as a consequence of the morphological evolution of the shallow tidal environment, generating slightly less frequent and longer, but stronger, resuspension events.

Furthermore, almost no correlation is shown to exist between durations and interarrival times of over-threshold exceedances and between intensities and interarrival times, whereas the intensity of peak excesses and duration are highly correlated. This confirms that resuspension events can be modelled as a 3-D marked Poisson process with marks (intensity and duration) mutually dependent but independent on the interarrival times in all the historical configurations of the Venice Lagoon. Moreover, a

comparison with the analysis of over-threshold BSS events shows that interarrival times, intensities and durations of both BSS and SSC events are mutually related but are complementary features because of the non-local dynamics due to advection and dispersion processes .

These findings, together with those obtained for BSS events (D'Alpaos et al., 2023), provide the basis to develop a theoretical framework for generating synthetic, yet statistically realistic, forcings to be used in the long-term morphodynamic modelling of shallow tidal environments, in general, and for the Venice Lagoon, in particular.

Data availability. All data presented in this study and used for the analysis of the suspended sediment concentration are available at https://researchdata.cab.unipd.it/id/eprint/729 (10.25430/researchdata.cab.unipd.it.00000729)

Author contributions. Conceptualization: Davide Tognin, Andrea D'Alpaos, Andrea Rinaldo, Luca Carniello;

Methodology: Davide Tognin, Andrea D'Alpaos, Luca Carniello;

Formal analysis and investigation: Davide Tognin;

Figures: Davide Tognin;

Writing - original draft preparation: Davide Tognin;

Writing - review and editing: all authors;

Funding acquisition: Andrea D'Alpaos, Luca Carniello;

Resources: Andrea D'Alpaos, Luca Carniello, Luigi D'Alpaos, Andrea Rinaldo;

Supervision: Andrea D'Alpaos, Luca Carniello.

Competing interests. The authors declare no competing interests.

Acknowledgements. TThis scientific activity was partially performed within the Research Programme Venezia2021, with contributions from the Provveditorato for the Public Works of Veneto, Trentino Alto Adige and Friuli Venezia Giulia, provided through the concessionary of State Consorzio Venezia Nuova and coordinated by CORILA, Research Line 3.2 (PI A.D.), the 2019 University of Padova project (BIRD199419) 'Tidal network ontogeny and evolution: a comprehensive approach based on laboratory experiments with ancillary numerical modelling and field measurements' (PI L.C.), the University of Padova SID2021 project, 'Unraveling Carbon Sequestration Potential by Salt-Marsh Ecosystems' (P.I. A. D.), and the iNEST (Interconnected Nord-Est Innovation Ecosystem) project and received funding from the European Union Next-GenerationEU (National Recovery and Resilience Plan – NRRP, Mission 4, Component 2, – D.D. 1058 23/6/2022, ECS00000043 - CUP: C43C22000340006).

References

Allen, J. I., Somerfield, P. J., and Gilbert, F. J.: Quantifying uncertainty in high-resolution coupled hydrodynamic-ecosystem models, Journal of Marine Systems, 64, 3–14, https://doi.org/10.1016/j.jmarsys.2006.02.010, 2007.

Amos, C. L., Bergamasco, A., Umgiesser, G., Cappucci, S., Cloutier, D., Denat, L., Flindt, M., Bonardi, M., and Cristante, S.: The stability of tidal flats in Venice Lagoon - The results of in-situ measurements using two benthic, annular flumes, Journal of Marine Systems, https://doi.org/10.1016/j.jmarsys.2004.05.013, 2004.

Anderson, F. E.: Resuspension of estuarine sediments by small amplitude waves, Journal of Sedimentary Research, 42, 602–607, 1972.

Balkema, A. A. and de Haan, L.: Residual Life Time at Great Age, The Annals of Probability, https://doi.org/10.1214/aop/1176996548, 1974.

Botter, G., Basso, S., Rodriguez-Iturbe, I., and Rinaldo, A.: Resilience of river flow regimes, Proceedings of the National Academy of Sciences, 110, 12 925–12 930, https://doi.org/10.1073/pnas.1311920110, 2013.

Brand, E., Chen, M., and Montreuil, A.-L.: Optimizing measurements of sediment transport in the intertidal zone, Earth-Science Reviews, 200, 103 029, https://doi.org/10.1016/j.earscirev.2019.103029, 2020.

Breugem, W. A. and Holthuijsen, L. H.: Generalized Shallow Water Wave Growth from Lake George, Journal of Waterway, Port, Coastal, and Ocean Engineering, https://doi.org/10.1061/(asce)0733-950x(2007)133:3(173), 2007.

Carniello, L., Defina, A., Fagherazzi, S., and D'Alpaos, L.: A combined wind wave-tidal model for the Venice lagoon, Italy, Journal of Geophysical Research: Earth Surface, 110, 1–15, https://doi.org/10.1029/2004JF000232, 2005.

Carniello, L., Defina, A., and D'Alpaos, L.: Morphological evolution of the Venice lagoon: Evidence from the past and trend for the future, Journal of Geophysical Research, 114, F04 002, https://doi.org/10.1029/2008JF001157, 2009.

Carniello, L., D'Alpaos, A., and Defina, A.: Modeling wind waves and tidal flows in shallow micro-tidal basins, Estuarine, Coastal and Shelf Science, 92, 263–276, https://doi.org/10.1016/j.ecss.2011.01.001, 2011.

Carniello, L., Defina, A., and D'Alpaos, L.: Modeling sand-mud transport induced by tidal currents and wind waves in shallow microtidal basins: Application to the Venice Lagoon (Italy), Estuarine, Coastal and Shelf Science, 102-103, 105–115, https://doi.org/10.1016/j.ecss.2012.03.016, 2012.

Carniello, L., Silvestri, S., Marani, M., D'Alpaos, A., Volpe, V., and Defina, A.: Sediment dynamics in shallow tidal basins: In situ observations, satellite retrievals, and numerical modeling in the Venice Lagoon, Journal of Geophysical Research: Earth Surface, 119, 802–815, https://doi.org/10.1002/2013JF003015, 2014.

Carniello, L., D'Alpaos, A., Botter, G., and Rinaldo, A.: Statistical characterization of spatiotemporal sediment dynamics in the Venice lagoon, Journal of Geophysical Research: Earth Surface, pp. 1049–1064, https://doi.org/10.1002/2015JF003793, 2016.

Carr, J. A., D'Odorico, P., McGlathery, K. J., and Wiberg, P. L.: Stability and bistability of seagrass ecosystems in shallow coastal lagoons: Role of feedbacks with sediment resuspension and light attenuation, Journal of Geophysical Research: Biogeosciences, 115, https://doi.org/10.1029/2009JG001103, 2010.

Carr, J. A., D'Odorico, P., McGlathery, K. J., and Wiberg, P. L.: Spatially explicit feedbacks between seagrass meadow structure, sediment and light: Habitat suitability for seagrass growth, Advances in Water Resources, 93, 315–325, https://doi.org/https://doi.org/10.1016/j.advwatres.2015.09.001, 2016.

Chen, X., Zhang, C., Paterson, D. M., Townend, I., Jin, C., Zhou, Z., Gong, Z., and Feng, Q.: The effect of cyclic variation of shear stress on non-cohesive sediment stabilization by microbial biofilms: the role of 'biofilm precursors', Earth Surface Processes and Landforms, 44, 1471–1481, https://doi.org/10.1002/esp.4573, 2019.

Christiansen, T., Wiberg, P. L., and Milligan, T. G.: Flow and Sediment Transport on a Tidal Salt Marsh Surface, Estuarine, Coastal and Shelf Science, 50, 315–331, https://doi.org/10.1006/ecss.2000.0548, 2000.

Cramér, H. and Leadbetter, M. R.: Stationary and related stochastic processes, John Wiley & Sons, Ltd, New York, 1967.

D'Alpaos, A. and Marani, M.: Reading the signatures of biologic-geomorphic feedbacks in salt-marsh landscapes, Advances in Water Resources, 93, 265–275, https://doi.org/10.1016/j.advwatres.2015.09.004, 2016.

D'Alpaos, A., Lanzoni, S., Marani, M., and Rinaldo, A.: Landscape evolution in tidal embayments: Modeling the interplay of erosion, sedimentation, and vegetation dynamics, Journal of Geophysical Research, 112, F01 008, https://doi.org/10.1029/2006JF000537, 2007.

D'Alpaos, A., Mudd, S. M., and Carniello, L.: Dynamic response of marshes to perturbations in suspended sediment concentrations and rates of relative sea level rise, Journal of Geophysical Research: Earth Surface, 116, 1–13, https://doi.org/10.1029/2011JF002093, 2011.

D'Alpaos, A., Carniello, L., and Rinaldo, A.: Statistical mechanics of wind wave-induced erosion in shallow tidal basins: Inferences from the Venice Lagoon, Geophysical Research Letters, https://doi.org/10.1002/grl.50666, 2013.

D'Alpaos, A., Tognin, D., Tommasini, L., D'Alpaos, L., Rinaldo, A., and Carniello, L.: Statistical characterization of erosion and sediment transport mechanics in shallow tidal environments. Part 1: erosion dynamics, Authorea Preprints, 2023.

D'Alpaos, L.: Fatti e misfatti di idraulica lagunare. La laguna di Venezia dalla diversione dei fiumi alle nuove opere delle bocche di porto, Istituto Veneto di Scienze, Lettere e Arti, Venice, 2010.

Defina, A.: Two-dimensional shallow flow equations for partially dry areas, Water Resources Research, 36, 3251–3264, https://doi.org/10.1029/2000WR900167, 2000.

D'Odorico, P. and Fagherazzi, S.: A probabilistic model of rainfall-triggered shallow landslides in hollows: A long-term analysis, Water Resources Research, https://doi.org/10.1029/2002WR001595, 2003.

Dyer, K. R.: Sediment processes in estuaries: Future research requirements, Journal of Geophysical Research, 94, 14 327, https://doi.org/10.1029/JC094iC10p14327, 1989.

Dyer, K. R., Christie, M. C., Feates, N., Fennessy, M. J., Pejrup, M., and van der Lee, W.: An Investigation into Processes Influencing the Morphodynamics of an Intertidal Mudflat, the Dollard Estuary, The Netherlands: I. Hydrodynamics and Suspended Sediment, Estuarine, Coastal and Shelf Science, 50, 607–625, https://doi.org/10.1006/ecss.1999.0596, 2000.

Fagherazzi, S. and Wiberg, P. L.: Importance of wind conditions, fetch, and water levels on wave-generated shear stresses in shallow intertidal basins, Journal of Geophysical Research: Earth Surface, https://doi.org/10.1029/2008JF001139, 2009.

Fagherazzi, S., Kirwan, M. L., Mudd, S. M., Guntenspergen, G. R., Temmerman, S., D'Alpaos, A., Van De Koppel, J., Rybczyk, J. M., Reyes, E., Craft, C., and Clough, J.: Numerical models of salt marsh evolution: Ecological, geomorphic, and climatic factors, Reviews of Geophysics, https://doi.org/10.1029/2011RG000359, 2012.

Ferrarin, C., Tomasin, A., Bajo, M., Petrizzo, A., and Umgiesser, G.: Tidal changes in a heavily modified coastal wetland, Continental Shelf Research, 101, 22–33, https://doi.org/10.1016/j.csr.2015.04.002, 2015.

Finotello, A., Tognin, D., Carniello, L., Ghinassi, M., Bertuzzo, E., and D'Alpaos, A.: Hydrodynamic Feedbacks of Salt-Marsh Loss in the Shallow Microtidal Back-Barrier Lagoon of Venice (Italy), Water Resources Research, 59, e2022WR032 881, https://doi.org/https://doi.org/10.1029/2022WR032881, e2022WR032881 2022WR032881, 2023.

Friedrichs, C. T. and Madsen, O. S.: Nonlinear diffusion of the tidal signal in frictionally dominated embayments, Journal of Geophysical Research, 97, 5637, https://doi.org/10.1029/92jc00354, 1992.

655 Gallager, R. G.: Stochastic Processes: Theory for Applications, Cambridge University Press, https://doi.org/10.1017/CBO9781139626514, 2013.

Gartner, J. W.: Estimating suspended solids concentrations from backscatter intensity measured by acoustic Doppler current profiler in San Francisco Bay, California, Marine Geology, 211, 169–187, https://doi.org/10.1016/j.margeo.2004.07.001, 2004.

Goodwin, G. C. H., Marani, M., Silvestri, S., Carniello, L., and D'Alpaos, A.: Toward coherent space-time mapping of seagrass cover from 660 satellite data: example of a Mediterranean lagoon, EGUsphere, 2023, 1–32, https://doi.org/10.5194/egusphere-2022-1501, 2023.

Grass, A. J.: Initial Instability of Fine Bed Sand, Journal of the Hydraulics Division, 96, 619–632, https://doi.org/10.1061/JYCEAJ.0002369, 1970.

Green, M. O.: Very small waves and associated sediment resuspension on an estuarine intertidal flat, Estuarine, Coastal and Shelf Science, 93, 449–459, https://doi.org/10.1016/j.ecss.2011.05.021, 2011.

665 Green, M. O. and Coco, G.: Sediment transport on an estuarine intertidal flat: Measurements and conceptual model of waves, rainfall and exchanges with a tidal creek, Estuarine, Coastal and Shelf Science, https://doi.org/10.1016/j.ecss.2006.11.006, 2007.

Green, M. O. and Coco, G.: Review of wave-driven sediment resuspension and transport in estuaries, Reviews of Geophysics, 52, 77–117, https://doi.org/10.1002/2013RG000437, 2014.

Green, M. O., Black, K. P., and Amos, C. L.: Control of estuarine sediment dynamics by interactions between currents and waves at several 670 scales, Marine Geology, 144, 97–116, https://doi.org/10.1016/S0025-3227(97)00065-0, 1997.

Holthuijsen, L. H., Booij, N., and Herbers, T. H. C.: A prediction model for stationary, short-crested waves in shallow water with ambient currents, Coastal Engineering, 13, 23–54, https://doi.org/https://doi.org/10.1016/0378-3839(89)90031-8, 1989.

Hughes, Z. J.: Tidal Channels on Tidal Flats and Marshes, in: Principles of Tidal Sedimentology, edited by Davis, R. and Dalrymple, R., chap. 11, pp. 1–621, Springer, https://doi.org/10.1007/978-94-007-0123-6, 2012.

675 Kirwan, M. L. and Murray, A. B.: A coupled geomorphic and ecological model of tidal marsh evolution, Proceedings of the National Academy of Sciences of the United States of America, 104, 6118–6122, https://doi.org/10.1073/pnas.0700958104, 2007.

Lawson, S. E., Wiberg, P. L., McGlathery, K. J., and Fugate, D. C.: Wind-driven sediment suspension controls light availability in a shallow coastal lagoon, Estuaries and Coasts, 30, 102–112, https://doi.org/10.1007/BF02782971, 2007.

Le Hir, P., Monbet, Y., and Orvain, F.: Sediment erodability in sediment transport modelling: Can we account for biota effects?, Continental 680 Shelf Research, 27, 1116–1142, https://doi.org/10.1016/j.csr.2005.11.016, 2007.

Lesser, G., Roelvink, J., van Kester, J., and Stelling, G.: Development and validation of a three-dimensional morphological model, Coastal Engineering, 51, 883–915, https://doi.org/https://doi.org/10.1016/j.coastaleng.2004.07.014, coastal Morphodynamic Modeling, 2004.

Maciel, F. P., Santoro, P. E., and Pedocchi, F.: Spatio-temporal dynamics of the Río de la Plata turbidity front; combining remote sensing with in-situ measurements and numerical modeling, Continental Shelf Research, 213, 104 301, 685 https://doi.org/https://doi.org/10.1016/j.csr.2020.104301, 2021.

Marani, M., Da Lio, C., and D'Alpaos, A.: Vegetation engineers marsh morphology through multiple competing stable states, Proceedings of the National Academy of Sciences, https://doi.org/10.1073/pnas.1218327110, 2013.

Martini, P., Carniello, L., and Avanzi, C.: Two dimensional modelling of flood flows and suspended sedimenttransport: the case of the Brenta River, Veneto (Italy), Natural Hazards and Earth System Sciences, 4, 165–181, https://doi.org/10.5194/nhess-4-165-2004, 2004.

690   Masselink, G., Hughes, M., and Knight, J.: Introduction to Coastal Processes and Geomorphology, Routledge, https://doi.org/10.4324/9780203785461, 2014.

Mathew, R. and Winterwerp, J. C.: Morphodynamic modeling and morphological upscaling in a fine sediment system, Advances in Water Resources, 166, 104 224, https://doi.org/https://doi.org/10.1016/j.advwatres.2022.104224, 2022.

McSweeney, J. M., Chant, R. J., Wilkin, J. L., and Sommerfield, C. K.: Suspended-Sediment Impacts on Light-Limited Productivity in the
695   Delaware Estuary, Estuaries and Coasts, 40, 977–993, https://doi.org/10.1007/s12237-016-0200-3, 2017.

Mehta, A., Hayter, E. J., Parker, W. R., Krone, R. B., and Teeter, A. M.: Cohesive sediment transport. I: Process description, Journal of Hydraulic Engineering, 115, 1076–1093, 1989.

Miller, R. L. and McKee, B. A.: Using MODIS Terra 250 m imagery to map concentrations of total suspended matter in coastal waters, Remote Sensing of Environment, 93, 259–266, https://doi.org/https://doi.org/10.1016/j.rse.2004.07.012, 2004.

700   Möller, I., Spencer, T., French, J. R., Leggett, D. J., and Dixon, M.: Wave transformation over salt marshes: A field and numerical modelling study from north Norfolk, England, Estuarine, Coastal and Shelf Science, https://doi.org/10.1006/ecss.1999.0509, 1999.

Moore, K. A. and Wetzel, R. L.: Seasonal variations in eelgrass (Zostera marina L.) responses to nutrient enrichment and reduced light availability in experimental ecosystems, Journal of Experimental Marine Biology and Ecology, 244, 1–28, https://doi.org/https://doi.org/10.1016/S0022-0981(99)00135-5, 2000.

705   Murray, A. B.: Reducing model complexity for explanation and prediction, Geomorphology, 90, 178–191, https://doi.org/10.1016/j.geomorph.2006.10.020, 2007.

Nepf, H. M.: Drag, turbulence, and diffusion in flow through emergent vegetation, Water Resources Research, 35, 479–489, https://doi.org/10.1029/1998WR900069, 1999.

Nichols, M. M. and Boon, J. D.: Sediment Transport Processes in Coastal Lagoons, in: Coastal Lagoon Processes, edited by Kjerfve, B., C,
710   chap. 7, pp. 157–219, Elsevier, https://doi.org/10.1016/S0422-9894(08)70012-6, 1994.

Ouillon, S., Douillet, P., and Andréfouët, S.: Coupling satellite data with in situ measurements and numerical modeling to study fine suspended sediment transport: a study for the lagoon of New Caledonia, Coral Reefs, 23, 109–122, https://doi.org/10.1007/s00338-003-0352-z, 2004.

Park, J., Botter, G., Jawitz, J. W., and Rao, P. S. C.: Stochastic modeling of hydrologic variability of geographically isolated wetlands: Effects
715   of hydro-climatic forcing and wetland bathymetry, Advances in Water Resources, https://doi.org/10.1016/j.advwatres.2014.03.007, 2014.

Parker, G., Garcia, M., Fukushima, Y., and Yu, W.: Experiments on turbidity currents over an erodible bed, Journal of Hydraulic Research, 25, 123–147, https://doi.org/10.1080/00221688709499292, 1987.

Parsons, D. R., Schindler, R. J., Hope, J. A., Malarkey, J., Baas, J. H., Peakall, J., Manning, A. J., Ye, L., Simmons, S., Paterson, D. M., Aspden, R. J., Bass, S. J., Davies, A. G., Lichtman, I. D., and Thorne, P. D.: The role of biophysical cohesion on subaqueous bed form
720   size, Geophysical Research Letters, 43, 1566–1573, https://doi.org/10.1002/2016GL067667, 2016.

Pivato, M., Carniello, L., Moro, I., and D'Odorico, P.: On the feedback between water turbidity and microphytobenthos growth in shallow tidal environments, Earth Surface Processes and Landforms, 44, 1192–1206, https://doi.org/10.1002/esp.4567, 2019.

Puppin, A., Roner, M., Finotello, A., Ghinassi, M., Tommasini, L., Marani, M., and D'Alpaos, A.: Analysis of Organic Matter Decomposition in the Salt Marshes of the Venice Lagoon (Italy) Using Standard Litter Bags, Journal of Geophysical Research: Biogeosciences, 128,
725   e2022JG007 289, https://doi.org/https://doi.org/10.1029/2022JG007289, e2022JG007289 2022JG007289, 2023.

Ralston, D. K. and Stacey, M. T.: Tidal and meteorological forcing of sediment transport in tributary mudflat channels, Continental Shelf Research, 27, 1510–1527, https://doi.org/10.1016/j.csr.2007.01.010, 2007.

Rodriguez-Iturbe, I., Cox, D. R., and Isham, V.: Some models for rainfall based on stochastic point processes, Proceedings of the Royal Society of London. A. Mathematical and Physical Sciences, 410, 269–288, https://doi.org/10.1098/rspa.1987.0039, 1987.

730 Roelvink, J.: Coastal morphodynamic evolution techniques, Coastal Engineering, 53, 277–287, https://doi.org/https://doi.org/10.1016/j.coastaleng.2005.10.015, coastal Hydrodynamics and Morphodynamics, 2006.

Roner, M., D'Alpaos, A., Ghinassi, M., Marani, M., Silvestri, S., Franceschinis, E., and Realdon, N.: Spatial variation of salt-marsh organic and inorganic deposition and organic carbon accumulation: Inferences from the Venice lagoon, Italy, Advances in Water Resources, https://doi.org/10.1016/j.advwatres.2015.11.011, 2016.

735 Ruhl, C. A., Schoellhamer, D. H., Stumpf, R. P., and Lindsay, C. L.: Combined Use of Remote Sensing and Continuous Monitoring to Analyse the Variability of Suspended-Sediment Concentrations in San Francisco Bay, California, Estuarine, Coastal and Shelf Science, 53, 801–812, https://doi.org/10.1006/ecss.2000.0730, 2001.

Sanford, L. P.: Wave-Forced Resuspension of Upper Chesapeake Bay Muds, Estuaries, 17, 148, https://doi.org/10.2307/1352564, 1994.

Soulsby, R. L.: Bed shear-stresses due to combined waves and currents, in: Advances in Coastal Morphodynamics, edited by Stive, M. J. F.,

740 pp. 420–423, Delft Hydraul., Delft, Netherlands, 1995.

Soulsby, R. L.: Dynamics of Marine Sands: A Manual for Practical Applications, Thomas Telford, London, 1997.

Tambroni, N., Figueiredo da Silva, J., Duck, R. W., McLelland, S. J., Venier, C., and Lanzoni, S.: Experimental investigation of the impact of macroalgal mats on the wave and current dynamics, Advances in Water Resources, 93, 326–335, https://doi.org/10.1016/j.advwatres.2015.09.010, 2016.

745 Temmerman, S., Bouma, T. J., Govers, G., and Lauwaet, D.: Flow paths of water and sediment in a tidal marsh: Relations with marsh developmental stage and tidal inundation height, Estuaries, 28, 338–352, https://doi.org/10.1007/BF02693917, 2005.

Temmerman, S., Bouma, T. J., Van De Koppel, J., van der Wal, D., de Vries, M. B., and Herman, P. M. J.: Vegetation causes channel erosion in a tidal landscape, Geology, 35, 631–634, https://doi.org/10.1130/G23502A.1, 2007.

Tinoco, R. O. and Coco, G.: A laboratory study on sediment resuspension within arrays of rigid cylinders, Advances in Water Resources, 92,

750 1–9, https://doi.org/10.1016/j.advwatres.2016.04.003, 2016.

Tognin, D., D'Alpaos, A., Marani, M., and Carniello, L.: Marsh resilience to sea-level rise reduced by storm-surge barriers in the Venice Lagoon, Nature Geoscience, 14, 906–911, https://doi.org/10.1038/s41561-021-00853-7, 2021.

Tognin, D., Finotello, A., D'Alpaos, A., Viero, D. P., Pivato, M., Mel, R. A., Defina, A., Bertuzzo, E., Marani, M., and Carniello, L.: Loss of geomorphic diversity in shallow tidal embayments promoted by storm-surge barriers, Science Advances, 8, eabm8446,

755 https://doi.org/10.1126/sciadv.abm8446, 2022.

Tommasini, L., Carniello, L., Ghinassi, M., Roner, M., and D'Alpaos, A.: Changes in the wind-wave field and related salt-marsh lateral erosion: inferences from the evolution of the Venice Lagoon in the last four centuries, Earth Surface Processes and Landforms, 44, 1633–1646, https://doi.org/doi:10.1002/esp.4599, 2019.

Umgiesser, G., De Pascalis, F., Ferrarin, C., and Amos, C. L.: A model of sand transport in Treporti channel: northern Venice lagoon, Ocean

760 Dynamics, 56, 339–351, https://doi.org/10.1007/s10236-006-0076-z, 2006.

van Ledden, M., Wang, Z. B., Winterwerp, H., and De Vriend, H. J.: Sand-mud morphodynamics in a short tidal basin, in: Ocean Dynamics, https://doi.org/10.1007/s10236-003-0050-y, 2004.

van Rijn, L. C.: Sediment transport, part II: suspended load transport, Journal of hydraulic engineering, 110, 1613–1641, 1984.

Venier, C., D'Alpaos, A., and Marani, M.: Evaluation of sediment properties using wind and turbidity observations in the shallow tidal areas

765 of the Venice Lagoon, Journal of Geophysical Research: Earth Surface, https://doi.org/10.1002/2013JF003019, 2014.

Volpe, V., Silvestri, S., and Marani, M.: Remote sensing retrieval of suspended sediment concentration in shallow waters, Remote Sensing of Environment, 115, 44–54, https://doi.org/10.1016/j.rse.2010.07.013, 2011.

Vu, H. D., Wieşki, K., and Pennings, S. C.: Ecosystem engineers drive creek formation in salt marshes, Ecology, 98, 162–174, https://doi.org/10.1002/ecy.1628, 2017.

770   Wang, P.: Principles of Sediment Transport Applicable in Tidal Environments, in: Principles of Tidal Sedimentology, edited by Davis, R. A. and Dalrymple, R. W., vol. c, pp. 1–621, Springer Netherlands, Dordrecht, https://doi.org/10.1007/978-94-007-0123-6, 2012.

Widdows, J. and Brinsley, M.: Impact of biotic and abiotic processes on sediment dynamics and the consequences to the structure and functioning of the intertidal zone, Journal of Sea Research, 48, 143–156, https://doi.org/10.1016/S1385-1101(02)00148-X, 2002.

Woodroffe, C. D.: Coasts, Cambridge University Press, Cambridge, https://doi.org/10.1017/CBO9781316036518, 2002.

775   Wren, D. G., Barkdoll, B. D., Kuhnle, R. A., and Derrow, R. W.: Field Techniques for Suspended-Sediment Measurement, Journal of Hydraulic Engineering, 126, 97–104, https://doi.org/10.1061/(ASCE)0733-9429(2000)126:2(97), 2000.

Young, I. R. and Verhagen, L. A.: The growth of fetch limited waves in water of finite depth. Part 1. Total energy and peak frequency, Coastal Engineering, https://doi.org/10.1016/S0378-3839(96)00006-3, 1996.

Supplement for
Statistical characterization of erosion and sediment transport mechanics in shallow tidal environments. Part 2: suspended sediment dynamics

Davide Tognin[1,2,*], Andrea D'Alpaos[2,*], Luigi D'Alpaos[1], Andrea Rinaldo[1,3], and Luca Carniello[1]

[1]Department of Civil, Environmental, and Architectural Engineering, University of Padova, Padova, Italy
[2]Department of Geosciences, University of Padova, Padova, Italy
[3]Laboratory of Ecohydrology ECHO/IEE/ENAC, Ècole Polytechnique Fèdèrale de Lausanne, Lausanne, Switzerland
[*]These authors contributed equally to this work.

Correspondence: Davide Tognin (davide.tognin@unipd.it)

1 The Sediment Transport and Bed Evolution Module

1.1 The stochastic approach for the computation of the transport parameter

The transport parameter, T, is usually defined as

$$T = \max\left\{0; \frac{\tau_{wc}}{\tau_c} - 1\right\} \tag{1}$$

5   where τ_{wc} is the total bottom shear stress and τ_c is the critical shear stress for erosion. This definition describes a sharp transition between $T = 0$ and $T = \tau_{wc}/\tau_c - 1$ that cannot take into account the spatial and temporal variability of both τ_{wc} and τ_c in real tidal systems. Indeed, the bottom shear stress is very unsteady because of the non-uniform flow velocity, wave characteristics and small-scale bottom heterogeneity within a computational element, while the critical shear stress is also affected by the random grain exposure and bed composition in time and space.

10   Similarly to the stochastic approach proposed by Grass (1970), we assume that both bed shear stress, τ_{wc}, and critical shear stress, τ_c, are random and distributed according to a log-normal probability density function (Grass, 1970; Bridge and Bennett, 1992). Therefore, we can write

$$T = \frac{1}{\tau_c} \int_0^\infty \left[\int_{\tilde{\tau}_c}^\infty (\tilde{\tau_{wc}} - \tilde{\tau}_c) \cdot p_{wc}(\tilde{\tau_{wc}})d\tilde{\tau_{wc}}\right] \cdot p_c(\tilde{\tau}_c)d\tilde{\tau}_c \tag{2}$$

where $p_{wc}(\bullet)$ and $p_c(\bullet)$ are the probability density function of τ_{wc} and τ_c respectively, and $\tilde{\tau_{wc}}$, $\tilde{\tau}_c$ are the correspondent
15   dummy variables of integration.

The result of this stochastic approach is a smooth transition between $T = 0$ and $T = \tau_{wc}/\tau_c - 1$.

An adequate interpolation of Eq. 2, which is implemented in the numerical model, is given by

$$T = -1 + \left(1 + \left(\frac{\tau_b}{\tau_c}\right)^\varepsilon\right)^{1/\varepsilon} \tag{3}$$

where ε is a non-dimensional calibration parameter, that accounts for the shape of the log-normal distribution.

We report here as an example a comparison of the measured and computed SSC at the LT7 station (see Figure S2) for an intense north-easterly Bora wind event in April 2003 (Figure S3). Numerical simulations were performed either by using the classic formulation (Eq. 1) (black thin line) or computing T considering Eq. 3. Using the classic formulation, the model is not able to correctly compute the time evolution of the local turbidity at near-threshold conditions, especially at the beginning of the event (first peak on the 2nd April 2003). On the contrary, the agreement between measured and computed data is quite good when using the stochastic approach.

1.2 Model calibration

The calibration of the model was performed for different periods when SSC field measurements are available (Figure S2, but, for the sake of brevity, we report in the following some examples related to intense and weak resuspension events, referring the reader to Carniello et al. (2012) for a more detailed analysis. Model capability to capture the process is evaluated by means of the Nash-Sutcliffe Model Efficiency (NSE) (Allen et al., 2007).

Focusing on intense resuspension events, we report in the following the results of three periods characterized by intense wind speed, namely: i) 2–5 April 2003 characterized by Bora wind with speeds up to 16 m/s; ii) 9–13 December 2005 characterized by Bora wind with speeds up to 20 m/s; iii) 29 July–2 August 2007 characterized by Bora wind with speeds up to 20 m/s. The comparison with measured data for simulations with an intense wind event in different stations located within the lagoon shows that the model performance to reproduce SSC is from very good to excellent ($\text{NSE}_{\text{mean}} = 0.70$, $\text{NSE}_{\text{median}} = 0.67$, $\text{NSE}_{\text{std}} = 0.13$). In these inner stations, the main contribution to SSC is provided by the mud fraction being negligible the sand content far from the inlets. Interestingly, the model not only correctly predicts the magnitude of the SSC but also captures its modulation induced by tidal level and wind-wave variations (Figure S4).

Additional tests were also carried out considering events characterized by very low wind speed. In particular, we report the results for the period 12-18 April 2006 when turbidity data at six stations close to three inlets are available. At these locations, the sand contribution to the computed SSC is relatively large and of the same order of magnitude as mud contribution (i.e. mud concentration ∼10 mg/l and sand concentration ∼2–3 mg/l) because close to the inlets the bed composition is richer in sand content than in the inner lagoon. Also in this case the model performance is rated from very good to excellent ($\text{NSE}_{\text{mean}} = 0.62$, $\text{NSE}_{\text{median}} = 0.59$, $\text{NSE}_{\text{std}} = 0.21$). The numerical model correctly reproduces SSC also in the case of very low wind velocity, when the measured SSC can be one order of magnitude lower than that measured with high wind speed (Figure S5).
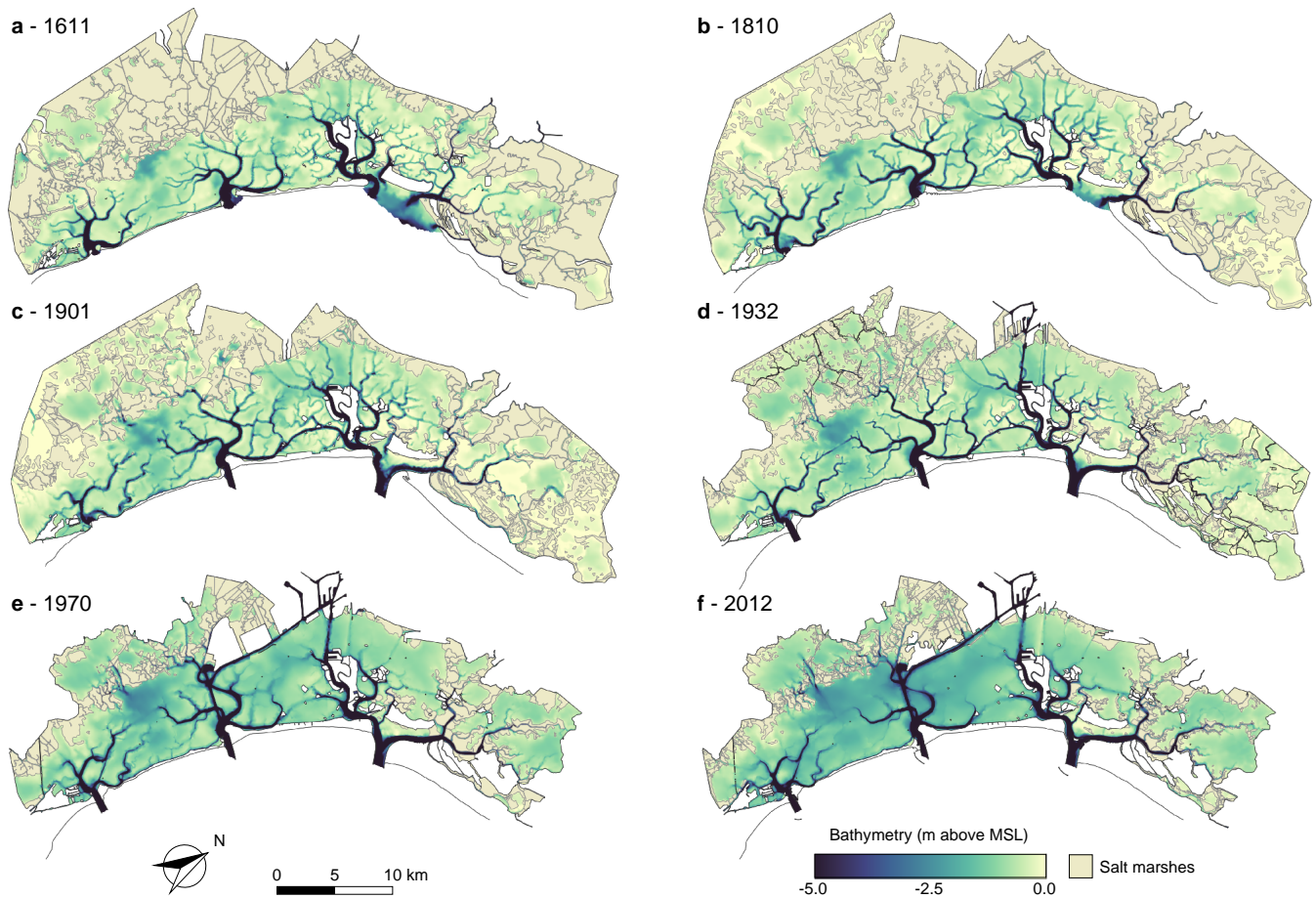
Figure S1. Historical bathymetries of the Venice Lagoon. Color-coded bathymetries of the six different configurations of the Venice Lagoon: (**a**) 1611, (**b**) 1810, (**c**) 1901, (**d**) 1932, (**e**) 1970, and (**f**) 2012. 1611 (a), 1810 (b), 1901 (c), 1932 (d), 1970 (e), and 2012 (f).
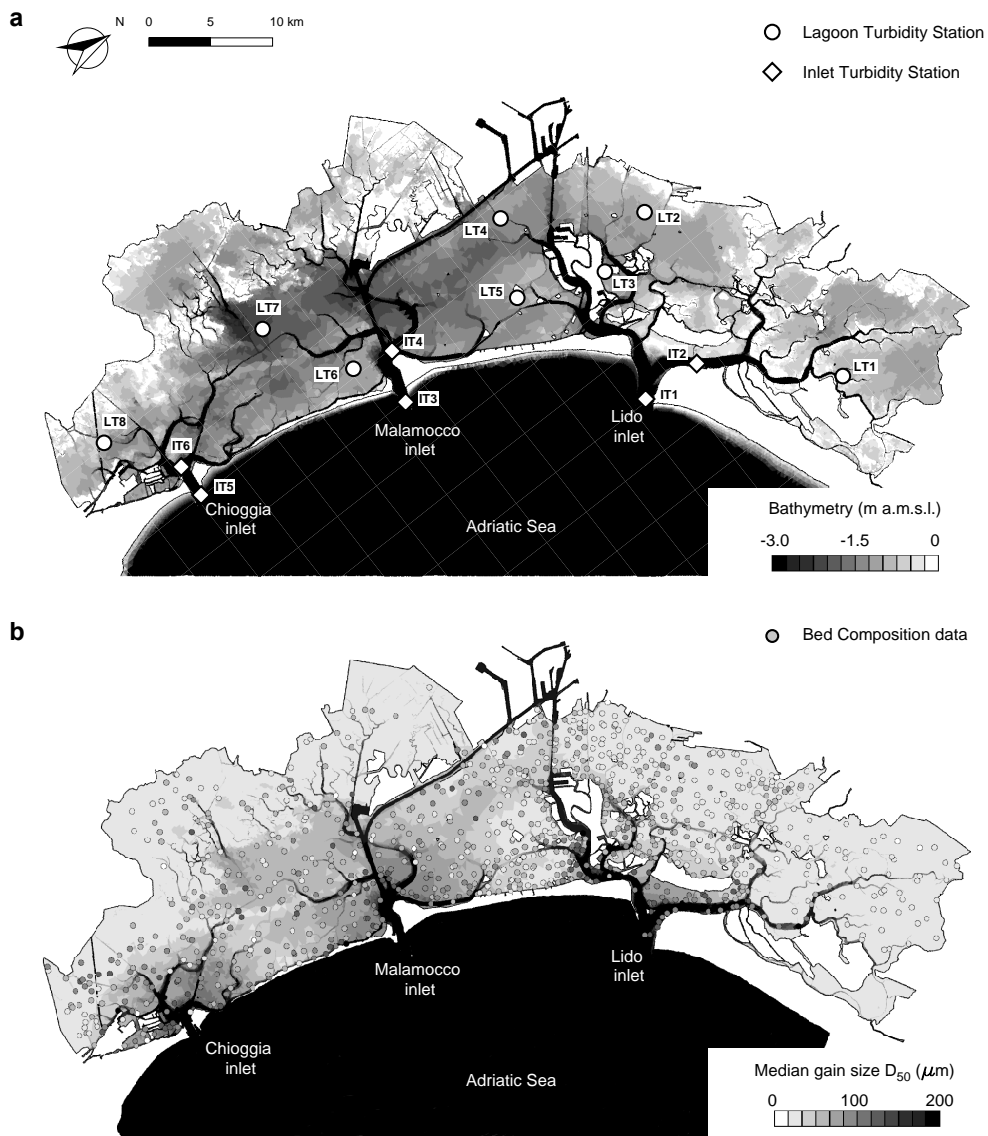
Figure S2. Turbidity and bed sediment grain size data. (**a**) Position of the turbidity stations within the Venice lagoon (LT) and at the inlets (IT). (**b**) Bed composition represented as median grain size D_{50} from measurements (dot) and interpolated (color-coded map).
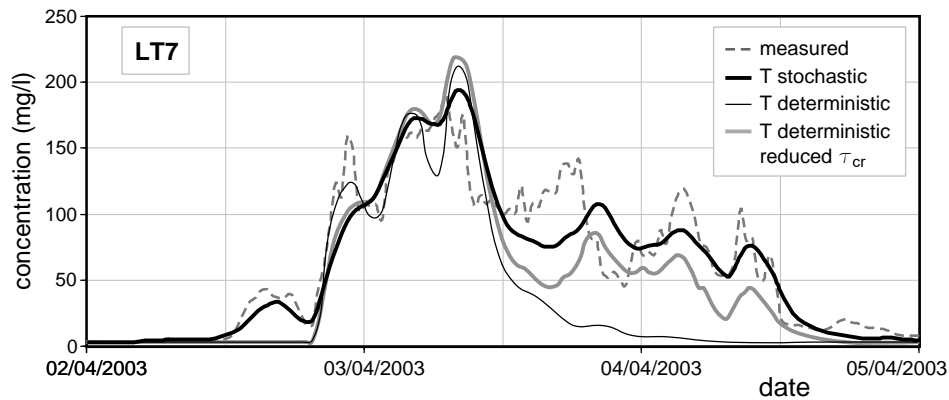
Figure S3. Stochastic approach for the computation of suspended sediment transport. Comparison of measured (dashed line) and computed (solid lines) suspended sediment concentration at the station LT7 (see Figure S2 for the location). The computed suspended sediment concentration was computed by estimating the transport parameter, T, (i) following the probabilistic approach (black bold line, Eq. 3; (ii) using the classic formulation (Eq. 1) without modifying the critical shear stress value (black thin line); (iii) using the classic formulation and reducing the critical shear stress value ($\tau_{cr,S} = 0.3$ Pa; $\tau_{cr,M} = 0.6$ Pa; grey line)
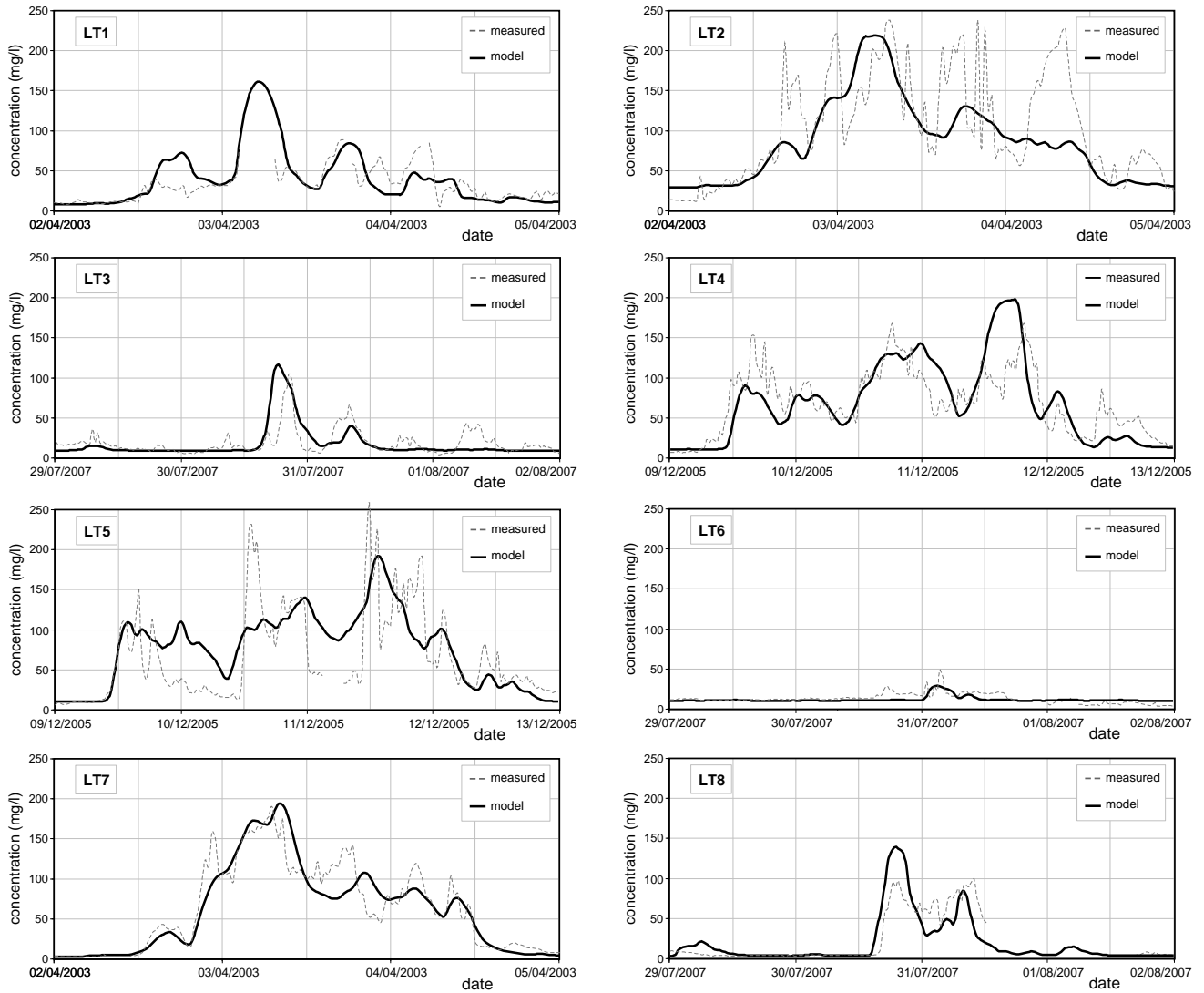
Figure S4. Sediment transport model calibration with intense wind events. Comparison of measured (dashed line) and computed (solid line) suspended sediment concentrations at the stations LT1 to LT8 within the lagoon during intense Bora wind events. See Figure S2 for the position of the stations.
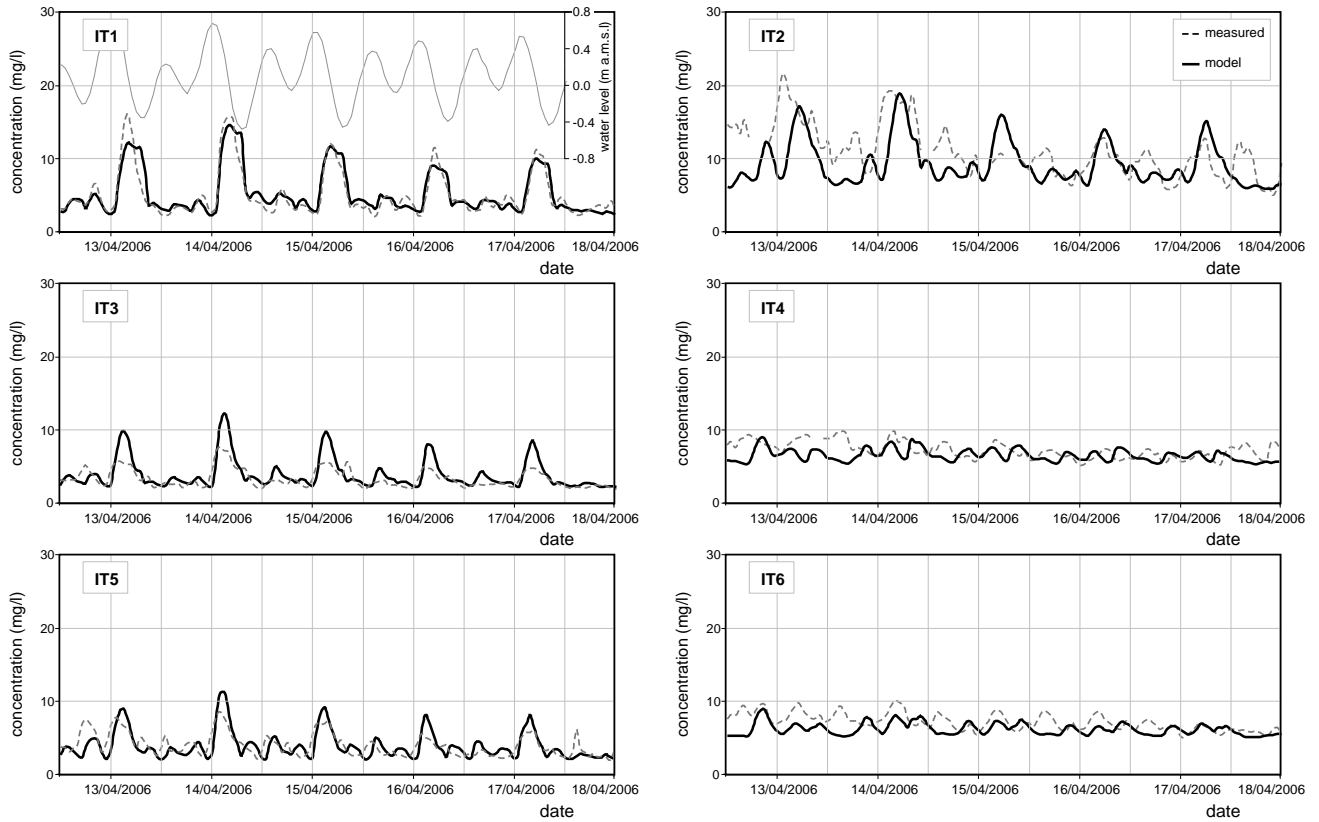
Figure S5. Sediment transport model calibration with weak wind conditions. Comparison of measured (dashed line) and computed (solid line) suspended sediment concentrations at the stations located close to the three inlets (IT) during an event characterized by very low wind conditions. The upper-left plot also shows the water level at the three inlets. See Figure S2 for the position of the stations.
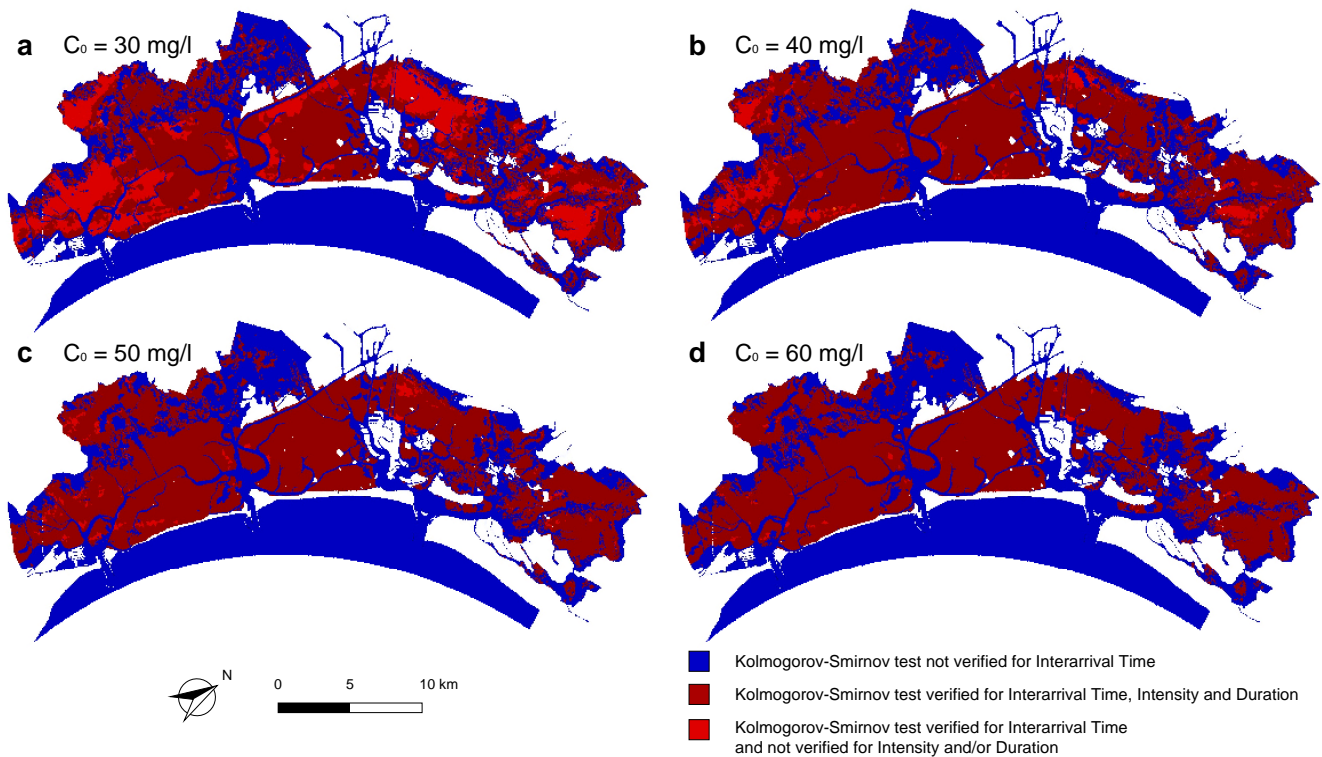
Figure S6. Sensitivity analysis of the threshold C_0**.** Spatial distribution of Kolmogorov-Smirnov (KS) test at significance level ($\alpha = 0.05$) for different values of the threshold, C_0: (**a**) 30 mg/l; (**b**) 40 mg/l; (**c**) 50 mg/l; (**d**) 60 mg/l. In the maps we can distinguish areas where the KS test is: not verified (dark blue); verified for all the considered stochastic variables (interarrival time, intensity over the threshold and duration) (dark red); verified for the interarrival time and not for intensity and/or duration (light red). Maps show little to no influence of the threshold value within the selected range on the possibility to model over-threshold SSC events as a Poisson process.
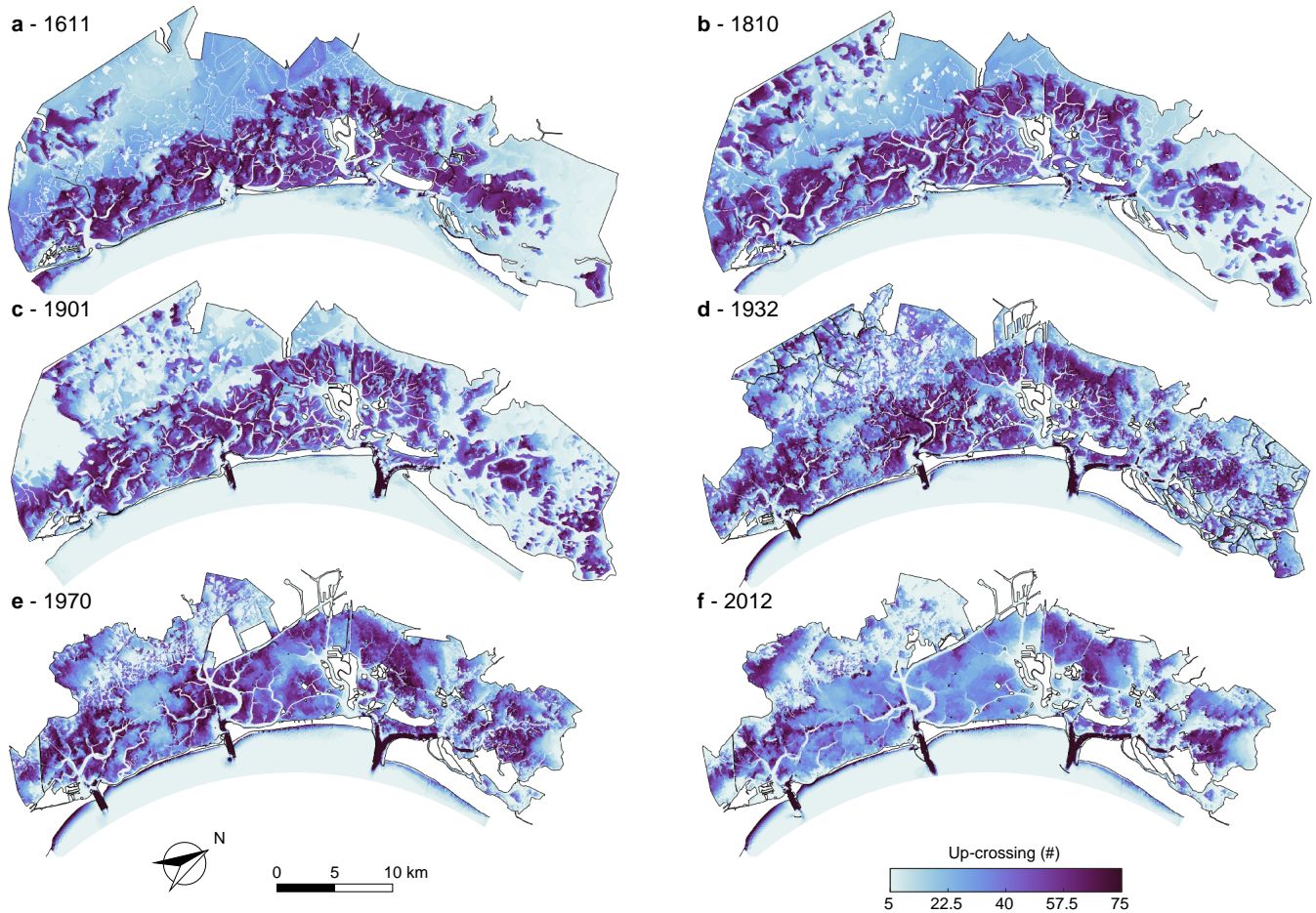
Figure S7. Number of upcrossings of the erosion threshold. Spatial distribution of the number of upcrossings of the threshold for erosion $\tau_c = 0.4$ Pa for the six different configurations of the Venice Lagoon: (a) 1611, (b) 1810, (c) 1901, (d) 1932, (e) 1970, and (f) 2012. ~~1611 (a), 1810 (b), 1901 (c), 1932 (d), 1970 (e), and 2012 (f).~~
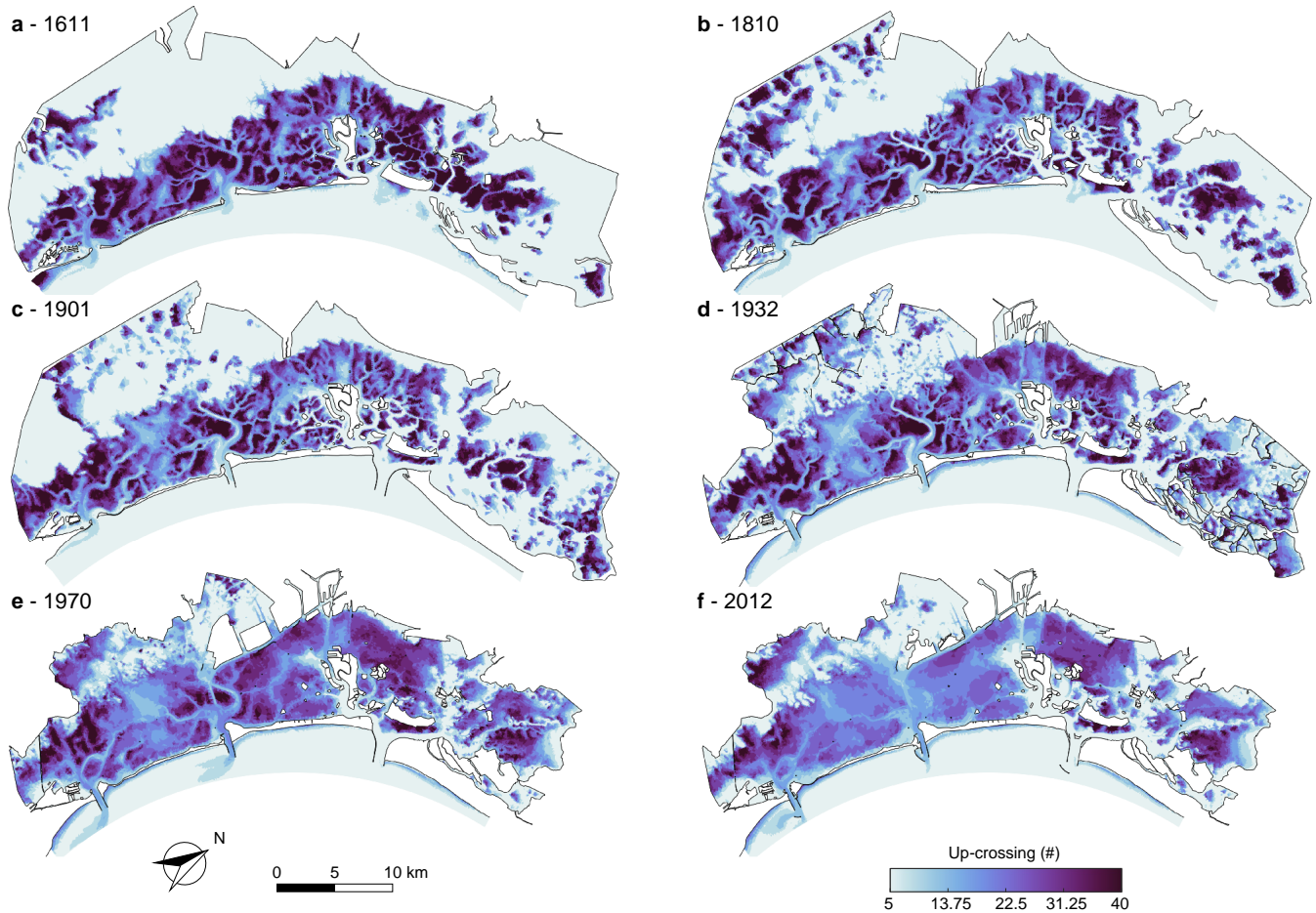
Figure S8. Number of upcrossings of the SSC threshold. Spatial distribution of the number of upcrossing of the threshold for suspended sediment concentration $C_0 = 40$ mg l^{-1}, for the six different configurations of the Venice Lagoon: (**a**) 1611, (**b**) 1810, (**c**) 1901, (**d**) 1932, (**e**) 1970, and (**f**) 2012. ~~1611 (**a**), 1810 (**b**), 1901 (**c**), 1932 (**d**), 1970 (**e**), and 2012 (**f**).~~
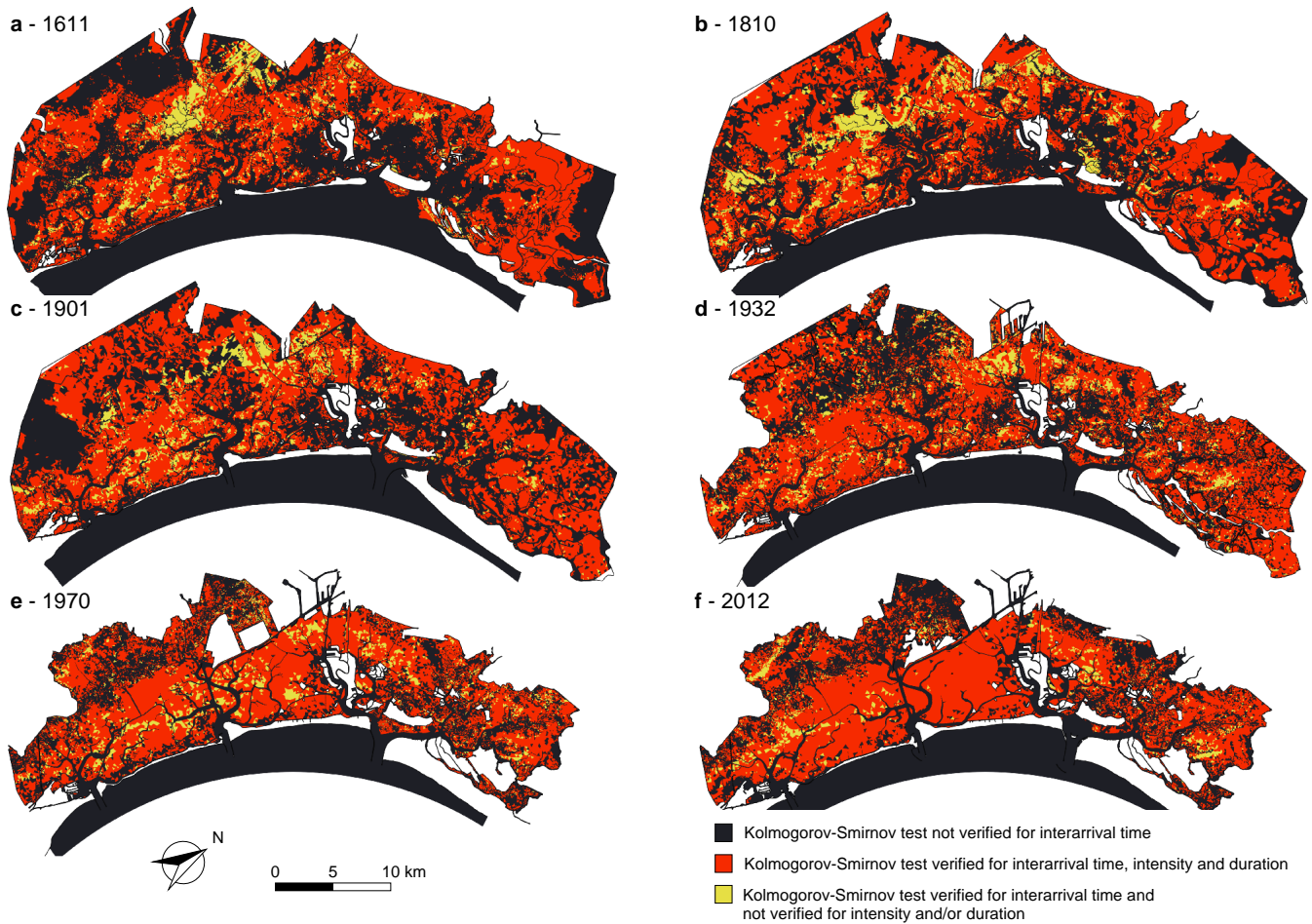
Figure S9. Kolmogorov-Smirnov test for over-threshold erosion events. Spatial distribution of Kolmogorov-Smirnov (KS) test at significance level ($\alpha = 0.05$) for the six different configurations of the Venice Lagoon: (a) 1611, (b) 1810, (c) 1901, (d) 1932, (e) 1970, and (f) 2012. ~~1611 (a), 1810 (b), 1901 (c), 1932 (d), 1970 (e), and 2012 (f).~~ In the maps we can distinguish areas where the KS test is: not verified (dark blue); verified for all the considered stochastic variables (interarrival time, intensity over the threshold and duration) (red); verified for the interarrival time and not for intensity and/or duration (yellow).

a
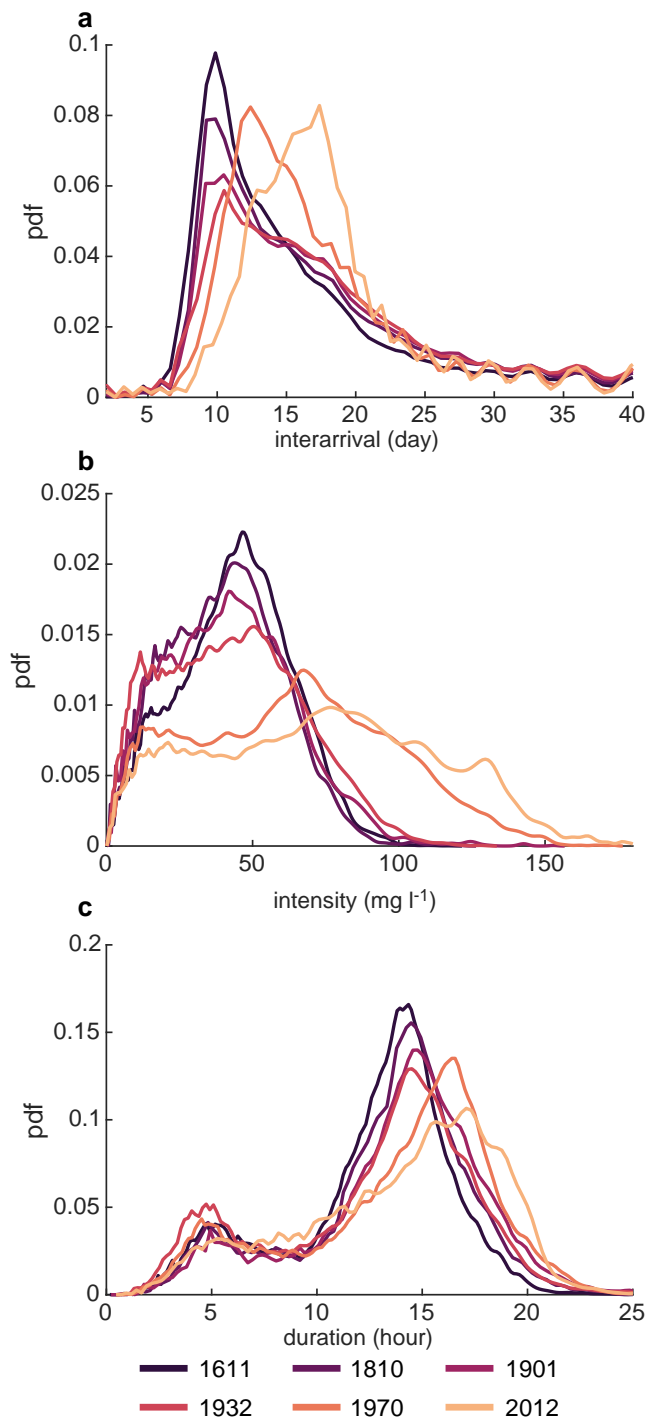
Year	t [day]	
	(mean $\pm$ std)	(median)
1611	27.49 ± 36.45	14.96
1810	29.35 ± 36.32	16.47
1901	32.47 ± 40.30	17.93
1932	33.59 ± 41.09	18.31
1970	27.87 ± 32.87	16.47
2012	29.24 ± 32.25	17.95

b

Year	e [mg l^{-1}]	
	(mean $\pm$ std)	(median)
1611	44.20 ± 19.00	44.99
1810	40.84 ± 19.17	41.05
1901	42.66 ± 21.80	41.96
1932	43.49 ± 23.36	42.95
1970	64.16 ± 33.86	65.02
2012	73.21 ± 38.85	74.68

c

Year	d [hour]	
	(mean $\pm$ std)	(median)
1611	12.58 ± 3.91	13.50
1810	13.23 ± 4.12	14.02
1901	13.78 ± 4.27	14.46
1932	12.71 ± 4.71	13.85
1970	13.76 ± 4.73	14.98
2012	13.96 ± 4.70	14.96

— 1611 — 1810 — 1901 — 1932 — 1970 — 2012

Figure S10. Spatial probability density function of interarrival time, intensity and duration of SSC over-threshold events. Probability density function (left), mean (mean $\pm$ standard deviation) and median value (right) of interarrival times t (**a**), intensity e (**b**) and duration d (**c**) of SSC over-threshold events.
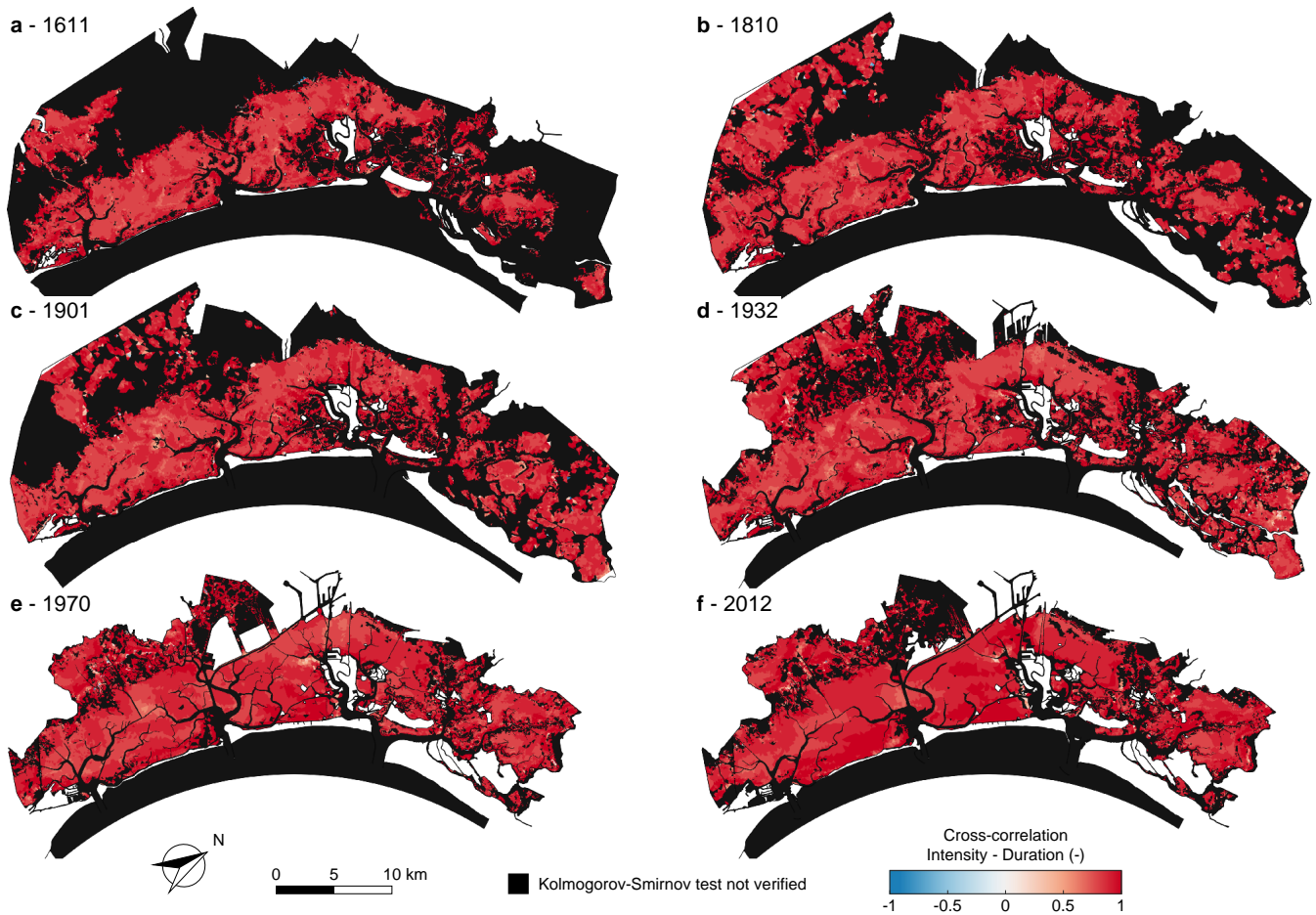
Figure S11. Cross-correlation between intensity and duration over-threshold SSC events. Spatial distribution of temporal cross-correlation between intensity of peak-excesses and duration of over-threshold exceedances for the six different configurations of the Venice Lagoon: (**a**) 1611, (**b**) 1810, (**c**) 1901, (**d**) 1932, (**e**) 1970, and (**f**) 2012. ~~1611 (**a**), 1810 (**b**), 1901 (**c**), 1932 (**d**), 1970 (**e**), and 2012 (**f**).~~ Black identifies sites where over-threshold SSC events cannot be modeled as a marked Poisson process (i.e. the KS test is not verified for the interarrival time).
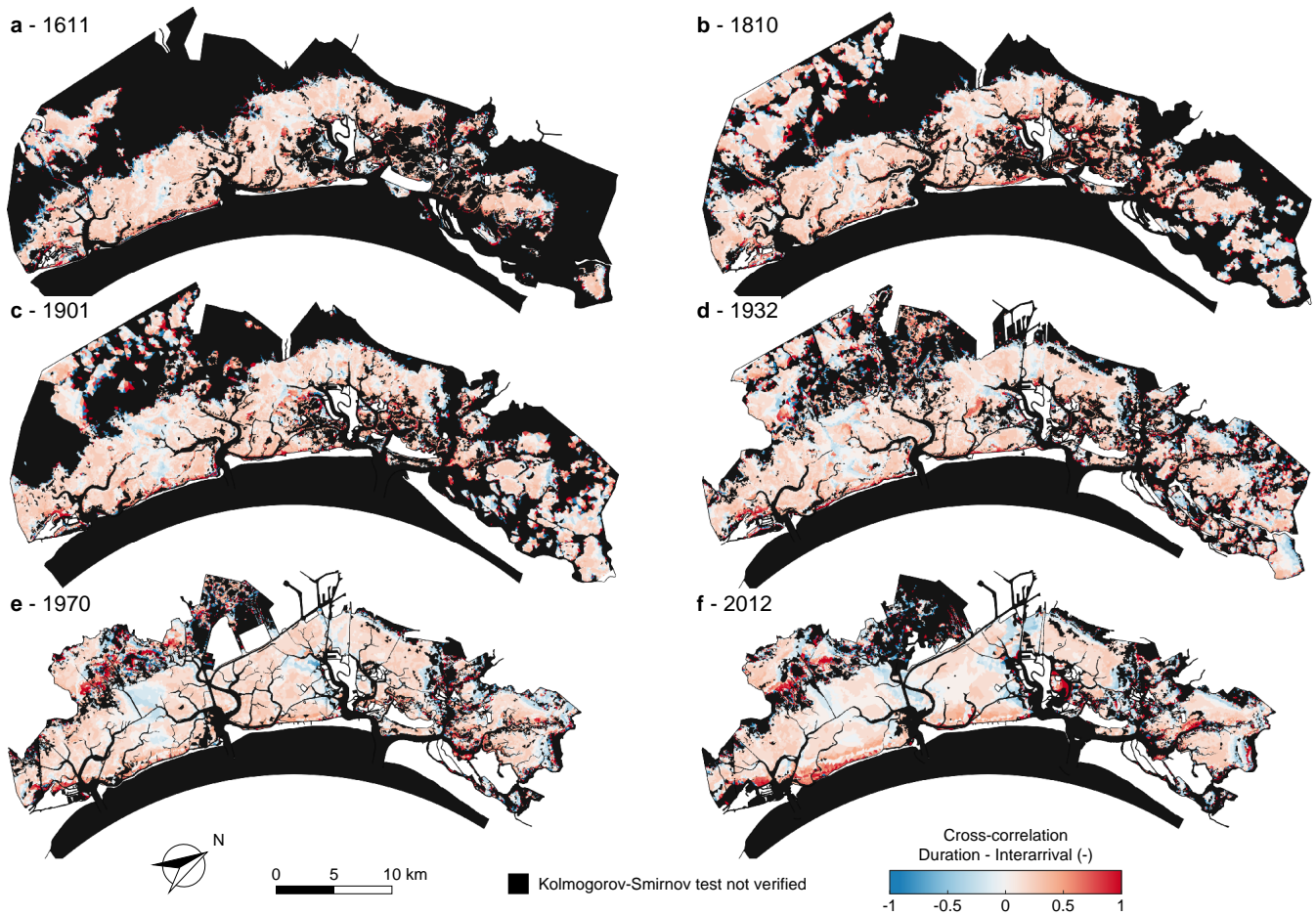
Figure S12. Cross-correlation between duration and interarrival times over-threshold SSC events. Spatial distribution of temporal cross-correlation between duration and interarrival times of over-threshold exceedances for the six different configurations of the Venice Lagoon: (a) 1611, (b) 1810, (c) 1901, (d) 1932, (e) 1970, and (f) 2012. ~~1611 (a), 1810 (b), 1901 (c), 1932 (d), 1970 (e), and 2012 (f).~~ Black identifies sites where over-threshold SSC events cannot be modeled as a marked Poisson process (i.e. the KS test is not verified for the interarrival time).
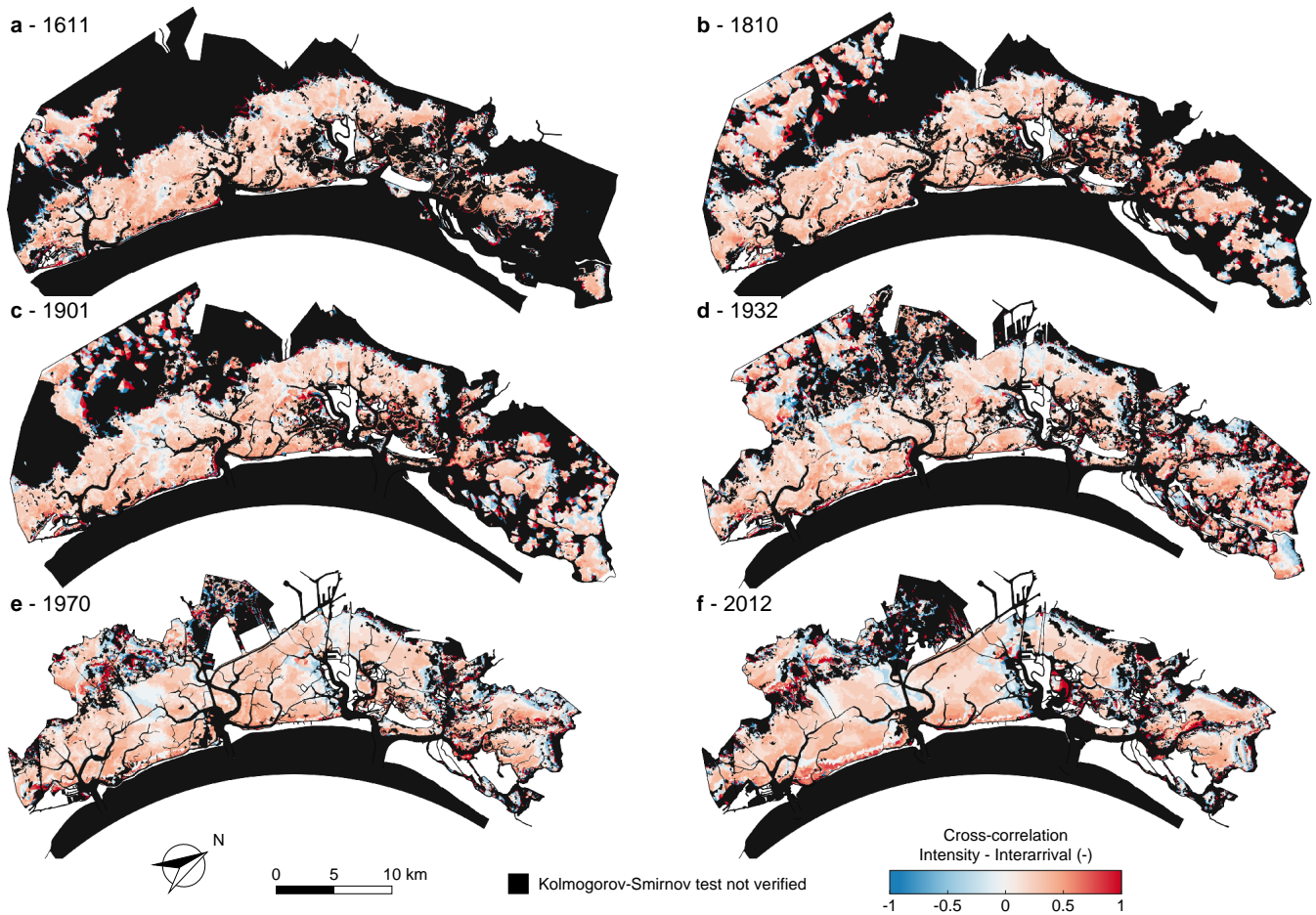
Figure S13. Cross-correlation between intensity and interarrival times of over-threshold SSC events. Spatial distribution of temporal cross-correlation between intensity of peak-excesses and interarrival times of over-threshold exceedances for the six different configurations of the Venice Lagoon: (a) 1611, (b) 1810, (c) 1901, (d) 1932, (e) 1970, and (f) 2012. ~~1611 (a), 1810 (b), 1901 (c), 1932 (d), 1970 (e), and 2012 (f).~~ Black identifies sites where over-threshold SSC events cannot be modeled as a marked Poisson process (i.e. the KS test is not verified for the interarrival time).

Year	$\rho(e-d)$ [-]
	(mean $\pm$ std)
1611	0.81 ± 0.10
1810	0.82 ± 0.11
1901	0.81 ± 0.11
1932	0.81 ± 0.12
1970	0.83 ± 0.10
2012	0.85 ± 0.10

Year	$\rho(t-d)$ [-]
	(mean $\pm$ std)
1611	0.14 ± 0.30
1810	0.15 ± 0.30
1901	0.13 ± 0.32
1932	0.12 ± 0.33
1970	0.11 ± 0.29
2012	0.10 ± 0.31

Year	$\rho(t-e)$ [-]
	(mean $\pm$ std)
1611	0.18 ± 0.30
1810	0.19 ± 0.31
1901	0.18 ± 0.33
1932	0.16 ± 0.34
1970	0.16 ± 0.30
2012	0.16 ± 0.32
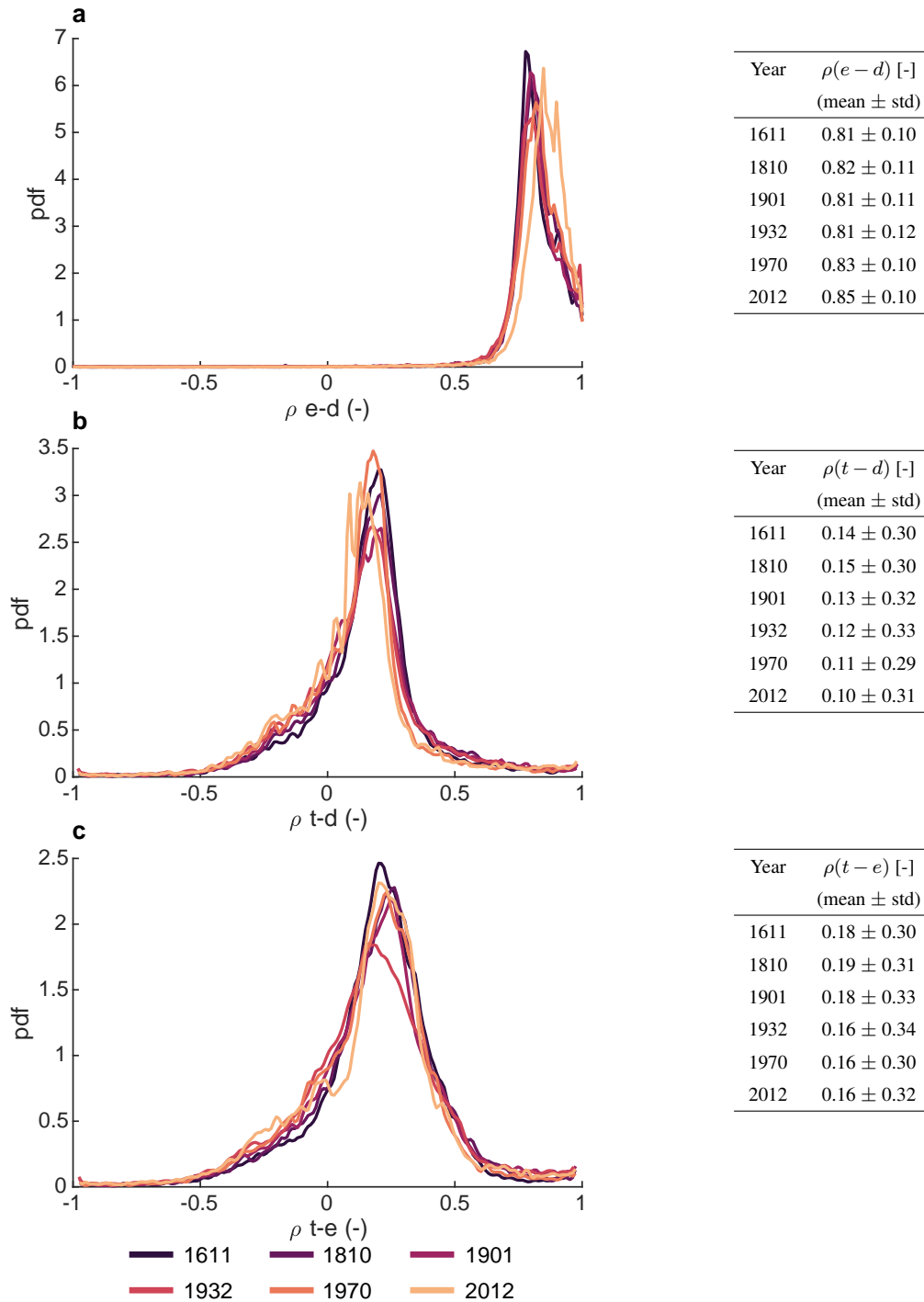
Figure S14. Spatial probability density function of cross-correlation between interarrival time, intensity and duration of SSC over-threshold events. Probability density function (left) and mean value (mean $\pm$ standard deviation, right) of cross-correlation between intesity and duration $\rho(e-d)$ (**a**), interarrival time and duration $\rho(t-d)$ (**b**) and interarrival time and intensity $\rho(t-e)$ (**c**).

References

Allen, J. I., Somerfield, P. J., and Gilbert, F. J.: Quantifying uncertainty in high-resolution coupled hydrodynamic-ecosystem models, Journal of Marine Systems, 64, 3–14, https://doi.org/10.1016/j.jmarsys.2006.02.010, 2007.

Bridge, J. S. and Bennett, S. J.: A model for the entrainment and transport of sediment grains of mixed sizes, shapes, and densities, Water Resources Research, 28, 337–363, https://doi.org/https://doi.org/10.1029/91WR02570, 1992.

Carniello, L., Defina, A., and D'Alpaos, L.: Modeling sand-mud transport induced by tidal currents and wind waves in shallow microtidal basins: Application to the Venice Lagoon (Italy), Estuarine, Coastal and Shelf Science, 102-103, 105–115, https://doi.org/10.1016/j.ecss.2012.03.016, 2012.

Grass, A. J.: Initial Instability of Fine Bed Sand, Journal of the Hydraulics Division, 96, 619–632, https://doi.org/10.1061/JYCEAJ.0002369, 1970.

50

55